

Appendix M

423708

A Three-Wave Model of the Stratosphere With Coupled Dynamics, Radiation and  
Photochemistry

R.-L. Shia, S. Zhou, M.K.W. Ko, N.-D. Sze, D. Salstein and  
K. Cady-Pereira



**A Three-Wave Model of the Stratosphere With Coupled Dynamics,  
Radiation and Photochemistry**

by

Run-Lie Shia, Shuntai Zhou<sup>+</sup>, Malcolm K. W. Ko, Nien-Dak Sze,  
David Salstein and Karen Cady-Pereira

Atmospheric and Environmental Research, Inc.  
840 Memorial Drive, Cambridge, MA 02139, USA

June 1997

<sup>+</sup> Now at the Climate Prediction Center, NWS, NOAA, Washington D. C.

## Abstract

A zonal mean chemistry transport model (2-D CTM) coupled with a semi-spectral dynamical model is used to simulate the distributions of trace gases in the present day atmosphere. The zonal-mean and eddy equations for the velocity and the geopotential height are solved in the semi-spectral dynamical model. The residual mean circulation is derived from these dynamical variables and used to advect the chemical species in the 2-D CTM. Based on a linearized wave transport equation, the eddy diffusion coefficients for chemical tracers are expressed in terms of the amplitude, frequency and growth rate of dynamical waves; local chemical loss rates; and a time constant parameterizing small scale mixing. The contributions to eddy flux are from the time varying wave amplitude (transient eddy), chemical reactions (chemical eddy) and small scale mixing. In spite of the high truncation in the dynamical module (only three longest waves are resolved), the model has simulated many observed characteristics of stratospheric dynamics and distribution of chemical species including ozone. Compared with the values commonly used in 2-D CTMs, the eddy diffusion coefficients for chemical species calculated in this model are smaller, especially in the subtropics. It is also found that the chemical eddy diffusion has only a small effects in determining the distribution of most slow species, including ozone in the stratosphere.

## 1. Introduction

Two-dimensional (zonal mean) chemistry transport models (CTMs) have played an important role in studying various physical and chemical processes which control the distributions of chemical constituents in the atmosphere. Comprehensive three-dimensional model with full chemistry is computationally too intensive to be used for long term (order of decades) simulation of the atmosphere. In addition, a zonal-mean approach provides an important alternative to interpreting the enormous amount of data from three-dimensional model and satellite observations. Therefore, the continuing improvements of two-dimensional models are indispensable.

This paper documents a highly truncated semi-spectral dynamical model coupled with a two-dimensional photochemistry transport model of the stratosphere. With small increases in computing resources, the approach described here provides the following improvements from traditional two-dimensional models in the calculation of dynamical variables, the transport of trace gases, and the interactions between the dynamics and tracer distribution:

- The primitive equations for the dynamical variables are separated into two sets, one for zonal-mean variables and one for eddies. Here, the word "eddy" refers to quantities that deviate from the zonal-mean. The eddy fluxes in the zonal mean momentum and thermodynamical equations represent transport of momentum and heat in the latitude-height plane due to zonally asymmetric motions and are calculated from resolved waves instead of using parameterization in terms of zonal-mean quantities. The three longest planetary waves are generated by imposing observed seasonally varying geopotential height at the lower boundary. Their propagation through the troposphere

into the stratosphere is calculated by the model. Kinnersley (1995) demonstrated that including wave-wave interactions is important in properly distributing energy among waves. Also included in the eddy equations is a linear damping term which represents the wave cascading to small unresolved scales. These small scale waves contribute to eddy mixing of chemical tracers when they are coupled with the planetary waves.

- The zonal-mean concentrations of the trace gases are obtained by solving the zonal-mean transport equation. Transport in the latitude-height plane of a 2-D CTM consists of the residual circulation and the eddy flux that represents net transport due to zonally asymmetric motions. The residual circulation is calculated directly according to its definition from the Eulerian mean velocity and eddy flux of temperature. The contribution of eddy fluxes to the zonal mean distribution of chemical tracers in the 2-D CTM module is parameterized as a diffusion flux with the diffusion coefficients calculated explicitly from the dynamical waves. The approach of calculating eddy diffusion coefficients is based on the linearized eddy tracer transport equation similar to that used by Pyle and Rogers (1980), Strobel (1981), and Smith and Brasseur (1990). With the contribution from small scale mixing and chemical eddy added to the transient eddy, the total eddy transport is mainly diffusive (down-gradient). The values of eddy diffusion coefficients are smaller than those commonly used in 2-D CTMs especially in the tropics.

- The model includes interactions between dynamics, radiation and chemistry. The chemical composition of the atmosphere can affect the dynamics by changing the heating/cooling rates through radiative transfer. Meanwhile, the dynamics can change the tracer distribution through changes in the residual mean circulation, zonal mean temperature and eddy diffusion coefficients.

The paper is organized as follows. Section 2 is a simple review of the eddy parameterization in 2-D CTMs. In Section 3 we give a brief description of the model, with emphasis on the dynamical module. The scheme of calculating eddy diffusion coefficients is formulated in Section 4. The model is used to simulate the present day atmosphere and the results for dynamical fields, the eddy diffusion coefficients and the distributions for trace gases, such as  $\text{N}_2\text{O}$ ,  $\text{CH}_4$  and  $\text{O}_3$ , are compared with observations and with previous studies in Section 5. Discussions of results are given in the last section.

## **2. Parameterization of Eddy Fluxes**

The transformed Eulerian mean (TEM) circulation in the pressure coordinates or the zonal-mean circulation in the isentropic coordinates have been extensively used in two-dimensional chemistry transport models. If the zonal asymmetric motion can be described by small amplitude steady adiabatic waves, these two circulations become identical and represent the Lagrangian mean motions of air parcels (Tung, 1984). The total transport of trace gases is represented by an advection due to the circulations and an eddy flux which is mainly diffusive. The circulations are driven by diabatic heating, dissipation and eddy forcing.

While it is commonly accepted that the eddy transport in the middle atmosphere is mainly due to organized planetary scale waves, rather than chaotic or turbulent mixing, there are still controversies about how to parameterize the eddy fluxes. A series of efforts to understand the mechanism of eddy transport and to derive the mixing coefficients began with Reed and German (1965). They parameterized the eddy fluxes in a two-dimensional model with Eulerian mean circulation as the product of a 2x2 diffusive

tensor and the gradient vector of zonal mean mixing ratio of tracers. However, due to an oversimplified assumption about the trajectories of air parcels, their results were later challenged. Matsuno (1980) showed that the trajectory of an air parcel driven by a steady planetary wave is elliptic when projected onto the meridional plane, and, therefore, there is no net transport for steady waves. Plumb (1979) and Pyle and Rogers (1980) reached the same conclusion using the linearized eddy tracer transport equation. Their results were the manifestation in Eulerian framework of the earlier study by Andrews and McIntyre (1978), which used the generalized Lagrangian mean formulation.

During the past several years, using more powerful computers and new numerical techniques, the problem of transport by planetary waves has been revisited by following trajectories of a large number of air parcels in the stratosphere or using the 'contour advection technique' (Schoeberl and Bacmeister, 1993; Bowman, 1993; Waugh and Plumb, 1994; Chen, 1994). These studies have provided intuitive pictures of eddy mixing. However, due to the lack of small scale mixing, these methods are useful only for simulations of a short time period. It is difficult to define directly from their results a parameterization of eddy mixing suitable for a global 2-D CTM.

The eddy flux for an inert tracer is given by the zonal mean of  $\overline{v' \cdot \chi'}$ , where  $v'$  is the eddy velocity in the meridional direction and  $\chi'$  is the eddy tracer distribution. For steady waves,  $v'$  and  $\chi'$  are orthogonal (90° phase lag between two waves) and the zonal-mean of their product, the eddy flux, is equal to zero. When the wave is not steady, the amplitude of  $\chi'$  changes with time. In this case, the phase relation between  $v'$  and  $\chi'$  changes due to the tendency term and/or chemical sink term in the wave equation and thus, generate net eddy flux. The eddy flux generated this way is related to the wave transience (transient eddy, Plumb, 1979) and chemical reactions (chemical eddy, Smith and Brasseur, 1990). Calculation of the transient eddy diffusion coefficient based on the

tracer wave equation have met with some conceptual and practical difficulties. It is easy to show that growing waves generate down-gradient eddy flux, and so are diffusive. On the other hand, decaying waves produce up-gradient eddy flux, which can initiate numerical instability in model calculations. As decaying and growing phases occur alternatively in the atmosphere, they would cancel each other. However, diagnostic calculations using observed wind suggest that the eddy transport is almost always diffusive (e. g. Plumb and Mahlman, 1987).

A popular parameterization scheme uses the flux-gradient relation of potential vorticity (PV) to derive eddy diffusion coefficients ( $K_{yy}^q = -\frac{\overline{v' \cdot q'}}{\partial \bar{q} / \partial y}$ ) either from observed or from model-calculated (three-dimensional) wind fields (Tung, 1987; Hitchman and Brasseur, 1988; Newman et al., 1988; Yang et al., 1991). The derived eddy diffusion coefficient for PV,  $K_{yy}^q$ , is then applied to all chemical species. As will be shown in Section 4, the eddy diffusion coefficient for any tracer (including PV which is a dynamical tracer) has a dynamical component (which is the same for all tracers), and a chemical component (which is species dependent). Therefore, the derived  $K_{yy}^q$  are appropriate for other tracers only if the chemical eddy component of the eddy diffusion are small for PV and for chemical tracers. It is quite possible that using  $K_{yy}^q$  for chemical species could overestimate the eddy transport for long-lived species by including the 'chemical eddy' of PV. There are other difficulties in practice.  $K_{yy}^q$  calculated from observed winds will contain negative values at some time and locations. These have to be ignored and substituted with positive values in a model simulation. Typical values of calculated  $K_{yy}^q$  are as large as  $10^6$  m<sup>2</sup>/sec. When these large values are used in two-dimensional models, they tend to underestimate the meridian gradients for long-lived gases in the stratosphere.

Garcia (1991) suggested a new method to parameterize eddy mixing through planetary wave breaking in the stratosphere. The time dependent equation for the eddy quasi-geostrophic potential vorticity ( $q'$ ) is solved explicitly for a single planetary wave. The eddy equation contains dissipation terms representing damping by Rayleigh friction, Newtonian cooling and a separate linear term,  $-\delta q'$ , representing damping due to wave-breaking. The wave-breaking criterion is  $|q'_y|/\bar{q}_y \geq 1$ . The value for the damping rate,  $\delta$ , is calculated at every time step for each location as follows. It is set to zero if  $|q'_y|/\bar{q}_y < 1$ . In region where  $|q'_y|/\bar{q}_y \geq 1$ , the values for  $\delta$  are calculated from the wave activity equation to stop further increase of the wave activity density. Garcia showed that the eddy flux for PV,  $\overline{v'q'}$ , can be written in the form  $-K_{yy}^G \bar{q}_y$ , where

$$K_{yy}^G = \frac{\delta \overline{v'v'}}{k^2(\bar{u} - c)^2 + \delta^2}. \text{ This eddy diffusion coefficient is used in the transport equation}$$

for all tracers. When the zonal wind ( $\bar{u}$ ) equation is solved, he compute the EP flux divergence as the eddy potential vorticity directly from the solution of the wave equations in order to include the contributions not only from the wave breaking but also from other processes (e.g. thermal damping of the wave). Kinnersley and Harwood (1993) and Kinnersley (1995, 1996) modified Garcia's method in an isentropic two-dimensional model by solving the eddy Ertel potential vorticity equation for the three longest waves. A wave-breaking criterion similar to the one used in Garcia (1991) was applied to each of the three waves. A simple procedure was used to find the damping rate ( $\delta_m$ ) which is large enough to stop the growth of the wave where its breaking criterion is met. The resulting eddy diffusion coefficient is the sum of the contribution from 3 waves,

$$K_{yy}^K = \sum_{m=1}^3 \frac{\delta_m \overline{v'v'}}{k_m^2(\bar{u} - c_m)^2 + \delta_m^2}.$$

Our approach differs from the above approach in that, the eddy diffusion coefficients for each chemical tracer is derived directly from the time dependent wave transport equation for the tracer and are calculated using wave fields simulated in a semi-

spectral dynamical model. Therefore, it is not necessary to make the assumption that the eddy diffusion coefficients derived based on the flux-gradient relationship of PV can be used for chemical tracer.

### **3. Model description**

The overall model has three modules, a semi-spectral dynamical model, a radiative transfer code, and a 2-D CTM. The model has  $9.5^\circ$  resolution in latitude (19 boxes from pole to pole),  $\sim 3.5$  km resolution in altitude (half scale height), and the three longest zonal waves are calculated in the dynamical module. The 2-D CTM has 17 vertical layers (from the surface to  $\sim 60$  km) while the dynamical module includes seven extra layers to place the upper boundary at  $\sim 84$  km.

The three-wave model differs from most interactive 2-D models in that it uses a highly truncated three-dimensional dynamical module to calculate the zonal mean and wave fields. In the current version of the model, only the three longest planetary waves are included. The interactive coupling between the dynamics and the distribution of atmospheric constituents is achieved when the model-calculated  $O_3$  is used to compute the radiative heating rates. The model flow chart is shown in Fig. 1. Interactions between different processes and feedbacks can be identified by following arrows in that figure. The data are exchanged between the dynamical module, the radiative transfer module and the chemistry transport module every ten days.

#### **3.1 Dynamical Module**

The dynamical module is adopted from Schneider and Geller (1984). It is formulated in the primitive equation system and the vertical coordinate is  $z = H \cdot \ln(p_0/p)$ .

The zonal mean equations are

$$\partial_t \bar{u} + \bar{v} \left( \partial_y \bar{u} - f - \frac{\bar{u}}{a} \tan \theta \right) + \bar{w} \partial_z \bar{u} = -E_U + D_U - \beta_R \bar{u}, \quad (1)$$

$$\partial_t \bar{v} + \bar{u} \left( f + \frac{\bar{u}}{a} \tan \theta \right) = -\partial_y \bar{\phi} - E_V + D_V - \beta_R \bar{v}, \quad (2)$$

$$\partial_t \bar{\phi}_z + \bar{v} \partial_y \bar{\phi}_z + \bar{w} \partial_z \bar{\phi}_z + \bar{w} N^2 = \frac{\kappa}{H} \bar{J} - E_T + D_T, \quad (3)$$

$$\frac{1}{\cos \theta} \partial_y (\bar{v} \cos \theta) + \frac{1}{\rho_0} \partial_z (\rho_0 \bar{w}) = 0. \quad (4)$$

Here  $\partial$  denotes the partial derivative, e. g.  $\partial_t$  is the time derivative,  $u$ ,  $v$  and  $w$  are the components of the velocity,  $\phi$  is the geopotential, and  $\phi_z \equiv \partial_z \phi$ , which is proportional to the temperature,  $\theta$  is the latitude,  $a$  is the radius of the Earth,  $\rho_0$  is the reference air density,  $f$  is Coriolis parameter,  $N$  is the Brunt-Vaisalla frequency,  $H$  is the scale height, taken to be 7 km,  $\kappa=2/7$ ,  $\beta_R$  is the Rayleigh friction coefficient which is a function of altitude.  $J$  is the radiative heating.  $E_U$ ,  $E_V$  and  $E_T$  are eddy flux divergence,

$$E_U = \frac{1}{\cos \theta} \partial_y (\overline{u'v'} \cos \theta) + \frac{1}{\rho_0} \partial_z (\rho_0 \overline{u'w'}) - \frac{\overline{u'v'}}{a} \tan \theta, \quad (5)$$

$$E_V = \frac{1}{\cos \theta} \partial_y (\overline{v'v'} \cos \theta) + \frac{1}{\rho_0} \partial_z (\rho_0 \overline{v'w'}) + \frac{\overline{u'u'}}{a} \tan \theta, \quad (6)$$

$$E_T = \frac{1}{\cos \theta} \partial_y (\overline{v'\phi'_z} \cos \theta) + \frac{1}{\rho_0} \partial_z (\rho_0 \overline{w'\phi'_z}). \quad (7)$$

The equations for deviation from the zonal mean (eddy), denoted by a prime, are

$$\partial_t u' + \bar{u} \partial_x u' + v' \partial_y \bar{u} - f v' - \frac{\bar{u} v' + \bar{v} u'}{a} \tan \theta = -\partial_x \phi' - W_u + D_u - \beta_R u' \quad (8)$$

$$\partial_t v' + \bar{u} \partial_x v' + v' \partial_y \bar{v} + w' \partial_z \bar{v} + f u' + 2 \frac{\bar{u} u'}{a} \tan \theta = -\partial_y \phi' - W_v + D_v - \beta_R v' \quad (9)$$

$$\partial_t \phi'_z + \bar{u} \partial_x \phi'_z + v' \partial_y \bar{\phi}_z + w' \partial_z \bar{\phi}_z + w' N^2 = \frac{\kappa}{H} J' - W_T + D_T \quad (10)$$

$$\partial_x u' + \frac{1}{\cos \theta} \partial_y (v' \cos \theta) + \frac{1}{\rho_0} \partial_z (\rho_0 w') = 0. \quad (11)$$

where  $W_u$ ,  $W_v$  and  $W_T$  are the terms of second order in the eddy equations, which represent the wave-wave interactions.

$$W_u = \partial_x (u'^2) + \frac{1}{\cos \theta} \partial_y ((u'v' - \overline{u'v'}) \cos \theta) + \frac{1}{\rho_0} \partial_z (\rho_0 (u'w' - \overline{u'w'})) - \frac{u'v' - \overline{u'v'}}{a} \tan \theta, \quad (12)$$

$$W_v = \partial_x (u'v') + \frac{1}{\cos \theta} \partial_y ((v'^2 - \overline{v'^2}) \cos \theta) + \frac{1}{\rho_0} \partial_z (\rho_0 (v'w' - \overline{v'w'})) + \frac{u'^2 - \overline{u'^2}}{a} \tan \theta, \quad (13)$$

$$W_T = \partial_x (u' \phi'_z) + \frac{1}{\cos \theta} \partial_y ((v' \phi'_z - \overline{v' \phi'_z}) \cos \theta) + \frac{1}{\rho_0} \partial_z (\rho_0 (w' \phi'_z - \overline{w' \phi'_z})). \quad (14)$$

$D_u$ ,  $D_v$ ,  $D_T$  in Eqns. (1)-(3) and  $D_{u'}$ ,  $D_{v'}$ ,  $D_{T'}$  in Eqns. (8)-(10) represent sub-grid scale diffusion and a biharmonic diffusion is used along the latitude direction with time scale of 14 days for a 2  $\Delta y$ -wave and 200 days for a 4  $\Delta y$ -wave for  $D_u$ ,  $D_v$ ,  $D_T$  (Schneider and Geller, 1984).

In the stratosphere only a few planetary scale waves prevail according to the wave propagating theory (Charney and Drazin, 1961). Therefore, we keep the three largest zonal waves, i.e. wavenumber 1, 2 and 3 for all the variables in Eqns. (8)-(11) using Fourier expansion around the latitude circle,

$$\psi' = \sum_{m=1}^3 \psi_m(t, y, z) e^{ik_m x} ,$$

where  $\psi' = (u', v', w', \phi')$ ,  $k_m = \frac{m}{a \cdot \cos \theta}$ ,  $m$  is the wave number,  $\theta$  is the latitude and  $a$  is the radius of the earth. The Eqns. (8)-(11) then become the wave equations for the Fourier coefficients  $\psi_m$ 's (See Schneider and Geller, 1984 for the details). The  $\psi_m$ 's are complex numbers. Their magnitude measures wave amplitude and their argument is related to the wave phase angle. When expanded in Fourier series, the wave-wave interactions terms ( $W_u$ ,  $W_v$ ,  $W_T$ ) should contain terms in the form of  $\sum_{m,n=1}^{\infty} \psi_m \zeta_n$ , where  $\psi_m$ ,  $\zeta_n$  can take on  $u_m$ ,  $v_m$ ,  $w_m$  or  $\phi_{zm}$ . Since we are only solving for the first 3 waves, the summation has to be truncated at  $m, n = 3$ . We add to the right hand side of the wave form of Eqns. (8)-(10) a linear damping term ( $-\gamma_{ss} u_m$ ,  $-\gamma_{ss} v_m$ , and  $-\gamma_{ss} \phi_{zm}$  respectively) to parameterize the wave decay due to the wave-wave interactions with smaller unresolved waves (wavenumber  $m > 3$ ). The same damping rate is used for  $u'$ ,  $v'$  and  $\phi'_z$ . The damping time constant,  $\tau_{ss} = 1/\gamma_{ss}$ , is an adjustable parameter. Our results show that the value of 60 days gives a reasonable calculated distribution of wave amplitudes for geopotential height.

It should be pointed out that a severely truncated model may result in kinetic energy build-up on the shortest wave (O'Brien and Branscome, 1989; Zhou and Stone, 1993). This does not occur in our three-wave model because the model has relatively fine resolution in the meridional direction (9.5°) and large sub-grid scale diffusion.

The model's vertical resolution in the troposphere is too crude to generate stationary waves via surface topography. We specify the lower boundary condition for wave amplitudes and phases from a set of climatology data. The data are extracted from

an archive of monthly mean grid point analyses of meteorological data (See the appendix for details). We only specify the first three wave components of the monthly mean geopotential height (  $\phi$  ) at 850 mb, the lower boundary of the model. The amplitudes of wave geopotential height at the lower boundary are shown in Fig. 2 for January and July respectively. The monthly mean data are interpolated to each time step and at the bottom layer of the model when the wave equations are integrated. The zonal mean and wave equations are solved with a time step of 30 minutes.

### 3.2 Radiative Transfer Module

The radiative heating in the zonal mean thermodynamical Eqn. (3) is calculated every 10 days using a narrow-band radiative transfer scheme described by Wang and Ryan (1983). In the eddy thermodynamic Eqn. (10), we use a simple Newtonian cooling form to represent  $J'$ , i.e.  $J' = -\alpha T'$ . The Newtonian cooling coefficient  $\alpha(\theta, z)$  is calculated from the zonal mean radiative heating using

$$\alpha(\theta, z) = -\frac{J(\bar{T} + \Delta T, \theta, z) - J(\bar{T}, \theta, z)}{\Delta T},$$

with  $\Delta T$  taken to be 0.5 °K.

Radiative heating is not the dominant component of the heating rate in the troposphere. The release of latent heat during convection is more important. The model does not directly calculate the latent heat release. Instead, the Cunnold (1975) parameterization scheme is used to include all heating sources by introducing in the energy equation a term that represents relaxation towards a prescribed temperature field with a prescribed time constant. The time constant is specified as a function of altitude

only, which is 10 days at the surface, increased to 20 days at 10 km and kept equal to 20 day up to the tropopause. This constant is also used as the Newtonian cooling time constant in the troposphere to calculate  $J'$ .

### 3.3 Chemistry Transport Module

As in most 2-D chemistry transport models, the grouping technique is used in the chemistry transport module of the three-wave model. All the fast chemical species are assumed in the local photochemical equilibrium state and are not transported individually. They are grouped into families. Each family species is transported with the appropriate net production and removal rate for the group. Our model includes 19 slow species ( $\text{N}_2\text{O}$ ,  $\text{CH}_4$ ,  $\text{C}_2\text{H}_6$ ,  $\text{H}_2$ ,  $\text{CO}$ ,  $\text{CH}_3\text{Cl}$ ,  $\text{CCl}_4$ ,  $\text{CFCl}_3$ ,  $\text{CF}_2\text{Cl}_2$ ,  $\text{CH}_3\text{CCl}_3$ ,  $\text{CF}_2\text{O}$ ,  $\text{CH}_3\text{Br}$ ,  $\text{CHClF}_2$ ,  $\text{C}_2\text{Cl}_3\text{F}_3$ ,  $\text{CBrClF}_2$ ,  $\text{CBrF}_3$ ,  $\text{O}_3$ ,  $\text{HNO}_3$ ,  $\text{H}_2\text{O}$ ) and five family species ( $\text{NO}_y$ ,  $\text{Cl}_y$ ,  $\text{Br}_y$ ,  $\text{F}_y$ ,  $\text{NO}_z = \text{NO}_y - \text{HNO}_3$ ).

The zonal mean transport equation for a slow species or a family species is

$$\partial_t \bar{\chi} + \bar{v}^* \partial_y \bar{\chi} + \bar{w}^* \partial_z \bar{\chi} = \bar{S} - \bar{\gamma} \cdot \bar{\chi} - \nabla \cdot \bar{F}$$

$$-\frac{1}{\rho_0} \partial_z \left[ \frac{\rho_0}{N^2} \overline{v' \phi'_z} \right] \frac{\partial \bar{\chi}}{\partial y} + \frac{1}{\cos \theta} \partial_y \left[ \frac{\cos \theta}{N^2} \overline{v' \phi'_z} \right] \frac{\partial \bar{\chi}}{\partial z}$$

(15)

where  $\bar{\chi}$  is the zonal-mean mixing ratio of chemical species,  $\bar{S}$  denotes the zonal-mean production rate,  $\bar{\gamma} \cdot \bar{\chi}$  is the zonal-mean removal rate. Here we have neglected the second-order term  $\overline{\gamma' \cdot \chi'}$ , which is assumed to be smaller than  $\bar{\gamma} \cdot \bar{\chi}$ .

In Eqn. (15),  $\bar{v}^*$  and  $\bar{w}^*$  are velocities of the residual mean meridional circulation, defined as

$$\begin{aligned}\bar{v}^* &= \bar{v} - \frac{1}{\rho_0} \partial_z \left( \frac{\rho_0}{N^2} \overline{v' \phi'_z} \right), \\ \bar{w}^* &= \bar{w} + \frac{1}{\cos \theta} \partial_y \left( \frac{\cos \theta}{N^2} \overline{v' \phi'_z} \right),\end{aligned}\tag{16}$$

and  $\bar{F}$  is the eddy flux,

$$\bar{F} = (\overline{v' \cdot \chi'}, \overline{w' \cdot \chi'}).\tag{17}$$

We could solve Eqn. (15) using values for  $\bar{F}$  calculated from a numerical solution of the eddy equation for  $\chi'$ :

$$\partial_t \chi' + \bar{u} \partial_x \chi' + v' \partial_y \bar{\chi} + w' \partial_z \bar{\chi} = -\bar{\gamma} \cdot \chi' - \gamma' \cdot \bar{\chi} - \gamma_{ss} \chi' + S'.\tag{18}$$

Note that we added a small scale mixing term  $-\gamma_{ss} \chi'$  in the equation. This term represents damping of zonal asymmetry in the tracer distribution by short-waves working in connection with planetary scale waves (cf. Matsuno (1980)). Eqn. (18) can, in principle, be solved in spectral form to obtain eddy tracer distribution  $\chi'$ . However, in the dynamics module we don't directly calculate  $w'$ , which is needed in order to solve Eqn. (18). Also there are several numerical difficulties associated with this approach. Apart from the well known problems related to the spectral solutions of the continuity equation (Allen et al., 1991), including  $\gamma' \cdot \bar{\chi}$  and  $S'$  terms will couple the eddy transport equations for different species.

In this study, we take the alternative approach by recognizing that if we ignore the  $\gamma' \cdot \bar{\chi}$  and  $S'$  terms in Eqn. (18), Eqn. (17) can be written in the form (See e.g. Strobel's derivation using a linear wave (1981)),

$$\partial_t \bar{\chi} + \bar{v}^* \partial_y \bar{\chi} + \bar{w}^* \partial_z \bar{\chi} = \bar{S} - \bar{\gamma} \cdot \bar{\chi} + \nabla \cdot (\bar{K} \cdot \nabla \bar{\chi}), \quad (19)$$

where  $\bar{K}$ , the diffusion tensor, is approximately symmetric (See Tung 1984; Tung et al. 1985). Tung (1984) argued that the eddy transport in the stratosphere due to planetary waves is dominated by the mixing along isentropic surfaces. Because the isentropic surfaces are nearly horizontal, it is usually assumed that  $K_{yy}$  is equal to the diffusion coefficient along the isentropic surface and  $K_{yz}$ ,  $K_{zy}$  can be calculated as the projections of  $K_{yy}$  from the isentropic surface back to the pressure coordinates.

In order to solve Eqn. (19), the chemistry scheme from the AER two-dimensional chemical transport model (Ko et al. 1984, 1985, 1989; Weisenstein et al. 1993) is used to calculate the chemical source term  $\bar{S}$  and loss rates  $\bar{\gamma}$ . The same numerical scheme described in the 2-D CTM is used to solve the transport equation for trace gases with a time step of 8 hours. The residual circulation ( $\bar{v}^*$ ,  $\bar{w}^*$ ) is calculated according Eqns. (16) and (17), and the  $\overline{v' \phi_z'}$  term required is computed at each (dynamical) time step of half an hour and averaged over 10 days in the dynamical module. At the end of each 10 day period, they are sent, along with a set of  $\bar{v}$  and  $\bar{w}$ , to the chemistry transport module. The values of  $\bar{v}^*$  and  $\bar{w}^*$  are then formed using Eqns. (15) and (16). The values used in each eight hour time step are obtained by interpolating between  $\bar{v}^*$  and  $\bar{w}^*$  calculated 10 days apart.

The formulas for calculating the stratospheric  $K_{yy}$ , which describes mixing along isentropic surfaces, from dynamical wave components, chemical loss rates and small

scale mixing are given in the next section. A constant  $K_{ZZ}$  of  $10 \text{ m}^2/\text{s}$  in the troposphere,  $0.1 \text{ m}^2/\text{s}$  in the stratosphere, and  $1 \text{ m}^2/\text{s}$  in the mesosphere is used to parameterize the rapid mixing by convections and turbulence in the troposphere and gravity wave breaking in the mesosphere. To represent the fast turbulent mixing in the troposphere, a constant value of  $1.5 \times 10^6 \text{ m}^2/\text{s}$  is used for  $K_{yy}$  in the troposphere except along the tropopause, where the values for  $K_{yy}$  are adjusted to represent the exchange between the stratosphere and the troposphere (Shia et al., 1993). These diffusion coefficients, along with calculated residual mean circulation, are then used in the zonal mean chemical transport model to calculate the distribution of the trace gases.

#### 4. Eddy Diffusion Coefficients $K_{yy}$

Assuming that  $\chi'$  and the perturbations in the velocity,  $v'$  and  $w'$  can be represented by linear waves, with the same longitudinal and time dependencies, i.e.  $\propto \exp(-\alpha t + i(kx - \omega t))$ . Strobel (1981) showed that

$$\chi' = \frac{-v' \partial_y \bar{\chi} - w' \partial_z \bar{\chi}}{(\bar{\gamma} - \alpha) - i(\omega - k\bar{u})}, \quad (20)$$

and  $K_{yy}$  is the coefficient of  $\partial_y \bar{\chi}$  in  $\overline{v' \chi'}$ , given as

$$K_{yy} = \frac{\bar{\gamma} - \alpha}{(\bar{\gamma} - \alpha)^2 + (\omega - k\bar{u})^2} \overline{v' v'}. \quad (21)$$

We can generalize the expression for  $K_{yy}$  for the multi-wave case with small scale mixing if we assume that  $\chi'$ ,  $v'$  and  $w'$  share the same  $x$  and  $t$  dependencies,

$$f'(t, x, y, z) = \text{Re}\left(\sum_{m=1}^N f_m(t, y, z) e^{ik_m x}\right) = \text{Re}\left(\sum_{m=1}^N f_m(y, z) e^{-i(\omega_m - i\alpha_m)t} e^{ik_m x}\right), \quad (22)$$

where  $\alpha_m$  (wave decaying rate), and  $\omega_m$  (wave frequency) are functions of latitude and altitude only.  $\alpha_m$  is negative for a growing wave and is positive for a decaying wave.

The expression for  $\chi'$  analogous to Eqn. (20) in the multi-wave case and with small scale mixing is given by

$$\chi_m = \frac{-v_m \partial_y \bar{\chi} - w_m \partial_z \bar{\chi}}{(\bar{\gamma} + \gamma_{ss} - \alpha_m) - i(\omega_m - k_m \bar{u})} \quad (23)$$

By examining  $\overline{v' \chi'} = \frac{1}{2} \text{Re}(\sum_{m=1}^N \chi_m(t, y, z) v_m^*(t, y, z))$ , we obtain an expression for  $K_{yy}$  as following,

$$K_{yy}^{tot} = \sum_{m=1}^3 \left( \frac{(\bar{\gamma} + \gamma_{ss} - \alpha_m) \cdot |v_m(t, y, z)|^2}{(\omega_m - k_m \bar{u})^2 + (\alpha_m - \bar{\gamma} - \gamma_{ss})^2} \right). \quad (24)$$

For diagnostic purpose, we define

$$K_{yy}^{tot} \equiv K_{yy}^{tr} + K_{yy}^{ch} + K_{yy}^{ss},$$

where

$$\begin{aligned} K_{yy}^{tr} &= \sum_{m=1}^3 \left( \frac{-\alpha_m \cdot |v_m(t, y, z)|^2}{(\omega_m - k_m \bar{u})^2 + (\alpha_m - \bar{\gamma}_{ch} - \gamma_{ss})^2} \right), \\ K_{yy}^{ch} &= \sum_{m=1}^3 \left( \frac{\bar{\gamma}_{ch} \cdot |v_m(t, y, z)|^2}{(\omega_m - k_m \bar{u})^2 + (\alpha_m - \bar{\gamma}_{ch} - \gamma_{ss})^2} \right), \\ K_{yy}^{ss} &= \sum_{m=1}^3 \left( \frac{\gamma_{ss} \cdot |v_m(t, y, z)|^2}{(\omega_m - k_m \bar{u})^2 + (\alpha_m - \bar{\gamma}_{ch} - \gamma_{ss})^2} \right). \end{aligned} \quad (25)$$

The truncating at wave number 3 is justified by assuming that the direct contribution from the smaller unresolved ( $m > 3$ ) waves to the global transport is

negligible compared with that from the planetary waves. However, the motions associated with wave number  $m > 3$  create small scale mixing which can be coupled with planetary waves to generate global scale mixing. The  $\gamma_{ss}$  is the damping rate for small scale mixing. We assume that this small scale mixing is related to the small scale mixing in Eqns. (8)-(10) in the dynamics model and the same time constant,  $\tau_{ss} = 1/\gamma_{ss}$ , of 60 days also should be used here for tracer mixing. This number is quite close to Matsuno's (1980) estimated value for small scale mixing of  $10^7$  sec.

The  $K_{yy}^{tr}$  defined in Eqn. (25) is the transient eddy coefficients. It is approximately proportional to the wave growing rate,  $-\alpha_m$ , which is species independent, and represents the mixing of inert gas by transient waves. This is consistent with the conclusion in Plumb (1979) and Pyle and Rogers (1980), that steady waves ( $\alpha_m = 0$ ) do not transport chemically inactive tracer. A growing wave ( $\alpha_m < 0$ ) implies positive  $K_{yy}^{tr}$ , giving rise to down-gradient transport. This kind of transport during wave growing periods was confirmed by observations (Leovy et al., 1985). After the wave reaches its peak, it decays ( $\alpha_m > 0$ ). For decaying period,  $K_{yy}^{tr}$  is less than zero and produces a up-gradient transport. The up-gradient transport in decaying period compensates the down-gradient transport in the precedent decaying period and generates little net transport. However, net transport results when the local tracer concentrations are changed by chemical reactions or by small scale mixing. They are represented by  $K_{yy}^{ch}$  and  $K_{yy}^{ss}$ , and both are always down-gradient (diffusive).

In order to determine  $K_{yy}$ , we need the wave frequency,  $\omega_m$  and wave decaying rate  $\alpha_m$ . They can be determined by

$$\frac{\partial_t v_m(t, y, z)}{v_m(t, y, z)} = -\alpha_m - i\omega_m, \quad (26)$$

using  $v_m$  calculated in the dynamics model. In doing so, we implicitly assume that one planetary wave is dominant in the zonal asymmetry with wave number equal to  $m$ . This is probably true in the region where the planetary waves are strong and generate large eddy mixing, which is what we are parameterizing. In the stratosphere, the typical time scale is about 10 days for  $\omega_m$  and several weeks for  $\alpha_m$ .

The diffusion coefficients,  $K_{yy}^{ir}$ ,  $K_{yy}^{ch}$ , and  $K_{yy}^{ss}$  are calculated in the dynamical module for every 30 minutes time step using Eqns. (25) and (26). The mean values of the eddy diffusion coefficients over the 10 day period are used in the transport equation for trace gases.

## 5. Model results

### 5.1 Dynamical Variables

The calculated global distributions for mean zonal wind and zonally averaged temperature for January and July are shown in Fig. 3. The magnitudes and locations of the polar jets in the winter hemisphere are in good agreement with observations (e. g., Barnett and Corney, 1985). The seasonal changes of subtropical tropospheric jets are also well simulated. However, the upper easterly in the summer hemisphere are weaker than observations. The winter zonal mean temperature in the polar lower stratosphere is more than  $10^\circ$  colder than observations. This problem is common in models with moderate resolution.

The latitude-height section of wave amplitude of wave 1, 2 and 3 calculated by the model and from the Climate Diagnostics Data Base (CDDDB; see the Appendix) data

for January and July are plotted in Fig. 4. In general, the model simulates the wave amplitudes well except that the amplitude of wave 1 is much smaller than the observations during winter in Northern Hemisphere. The parameterization of the heating rates in the troposphere limits the interaction between the troposphere and the stratosphere and may distort the wave propagation. Since the stratospheric waves propagate from the troposphere, the very strong hemispheric asymmetry of eddy activity in the stratosphere is mainly attributed to the specified lower boundary conditions. For the CDDB data, which we have used to prescribe geopotential height, waves are much weaker in the southern hemisphere winter than in the northern hemisphere winter, especially for wavenumbers 2 and 3 (Fig. 2).

## 5.2 Residual Mean Circulation

We calculate the residual mean circulation from the Eulerian mean circulation and eddy heat fluxes explicitly, according to Eqns. (16) and (17). The stream functions of residual mean meridional circulation are shown in Fig. 5 for four seasons. The stream patterns are very similar to those used in the TEM models or from the diabatic circulation (e.g., Hitchman and Brasseur, 1988; Ko et al., 1985). The upwelling motion occurs in the tropics and summer subtropics, and downward motion in the winter hemisphere. For spring and fall, the downward motion occurs in both hemispheres. These are the features of diabatic circulation. There has been some concern about the accuracy of the residual circulation calculated directly from Eqns. (16) and (17) due to the cancellation of the two terms on the r.h.s. of the equations. It is apparent from our model results that this is not a serious problem to affect the accuracy.

## 5.3 Eddy Diffusion Coefficients

The calculated total eddy diffusion coefficient,  $K_{yy}^{tot}$  for ozone and eddy diffusion coefficient for an inert tracer, which is  $K_{yy}^{tr} + K_{yy}^{ss}$ , are plotted in Figs. 6 and 7 respectively. Their difference is the chemical eddy due to the local chemical reactions which ozone participates. Both coefficients are smaller than  $4 \times 10^5$  m<sup>2</sup>/sec in most areas and all seasons except in the northern middle latitudes during winter. The tropical stratosphere has very small eddy diffusion year around. Negative values of  $K_{yy}^{tot}$  are calculated for ozone only during spring in northern upper midlatitudes. The magnitude of the negative values of  $K_{yy}^{tot}$  is quite small. The time step in the numerical scheme for solving Eqn. (20) is made smaller when necessary to avoid negative mixing ratio in the presence of the negative  $K_{yy}^{tot}$ . As expected,  $K_{yy}^{tot}$  for ozone is larger than  $K_{yy}^{tot}$  for an inert tracer. Also,  $K_{yy}^{tot}$  for long-lived species, e. g. methane (not shown), is very close to  $K_{yy}^{tot}$  for inert tracer.

As a comparison, the values for  $K_{yy}^q$ , which is derived from the flux-gradient relationship of the potential vorticity, are calculated using the model calculated winds. The quasi-geostrophic potential vorticity and its eddy are calculated using the following expressions.

$$q = f + \partial_x v - \partial_y u + \frac{f}{\rho_0} \partial_z \left( \frac{\rho_0 \Theta}{\Theta_z} \right) \quad (30)$$

$$q' = \partial_x v' - \partial_y u' + \frac{f}{\rho_0} \partial_z \left( \frac{\rho_0 \Theta'}{\Theta_z} \right) \quad (31)$$

Here  $f$  is the Coriolis parameter,  $\rho_0$  is the reference air density, which is the function of  $z$  only, and  $\Theta$  is the potential temperature. Using the least-square method (Newman et al., 1988), the values of  $\overline{v' \cdot q'}$  and  $\bar{q}_y$  are used to derive  $K_{yy}^q$ .

$$K_{yy}^q = -\frac{\overline{v' \cdot q' \cdot \bar{q}_y}}{[\bar{q}_y]^2} . \quad (32)$$

The direct application of Eqn. (32) will give large negative values of  $K_{yy}^q$  in some regions where  $\bar{q}_y$  is close to zero and the eddy flux is up-gradient. Therefore, a lower limit of zero is applied when  $K_{yy}^q$  is used in the transport calculations.

Model calculated  $K_{yy}^q$  shown in Fig. 8 shares the same features with that in Newman et al. (1988), such as north-south asymmetry, the seasonal variation. But the details in two set of  $K_{yy}^q$  are quite different due to the different wind fields used to calculate the potential vorticity. We are more interested in the differences between the model calculated  $K_{yy}^q$  and  $K_{yy}^{tot}$  for ozone and other tracers, because both are calculated using the quantities generated in the same model. As displayed in Figs. 6, 7 and 8,  $K_{yy}^q$  is larger than the total eddy diffusion coefficient,  $K_{yy}^{tot}$  for ozone and for inert tracer. One feature is shared by all these eddy diffusion coefficients: small diffusion in subtropical stratosphere.

The sign of the transient eddy diffusion coefficient,  $K_{yy}^r$ , changes frequently, and  $K_{yy}^{ss}$  is always positive. Their magnitudes are comparable so the total eddy diffusion coefficients are mostly positive (Fig. 6 and 7).

#### 5.4 Long-lived Species

N<sub>2</sub>O, CH<sub>4</sub> are good tracers because their chemical reactions are slow in the stratosphere and their sources are at the surface. Their distributions in the stratosphere are indicative of transport processes. To evaluate how realistic the calculated residual mean circulation and eddy diffusion are, we compare the model results of N<sub>2</sub>O and CH<sub>4</sub>

with the UARS/CLAES (Kummer et al., 1993) and UARS/HALOE (Tuck et al., 1993) data. The data show that the mixing ratios of N<sub>2</sub>O and CH<sub>4</sub> have two important features. The first is a "double peak" structure in the upper stratosphere during the period from February to May. This feature is attributed to a strong tropical meridional circulation (Choi and Holton, 1991). The second is that the tropical maxima tend to lean toward the summer hemisphere. In the upper stratosphere the maximum location is about 30° away from the equator in solstices. From December to May the ridge leans toward south, while from June to November it leans toward north. The model calculated mixing ratios of N<sub>2</sub>O and CH<sub>4</sub> are shown in Figs. 9 and 10 respectively. The "double peak" structure only vaguely shows up in the model simulations in the upper stratosphere during the northern winter. However, the "leaning ridge" feature is apparent in the summer hemisphere for both species and the simulated positions of the "leaning ridge" are close to where they are observed.

Simulated distributions for both CH<sub>4</sub> and N<sub>2</sub>O have steep "slopes" and large meridional gradients in the extratropics. This feature is also seen in recent observations of N<sub>2</sub>O and CH<sub>4</sub> from UARS/CLAES (Fig. 11). It is noted that these features have not been successfully simulated by some two-dimensional models, probably due to large eddy diffusion used in these models. As a demonstration, the simulated CH<sub>4</sub> distributions for four seasons using  $K_{yy}^q$  is plotted in Fig. 12. They are more 'flat' compared with Fig. 11.

Because both N<sub>2</sub>O and CH<sub>4</sub> are long-lived constituents, they share the same mixing surfaces in the lower stratosphere. According to Plumb and Ko (1992), the correlation between two long-lived species is compact if the horizontal diffusion dominates the transport process. The correlation between N<sub>2</sub>O and CH<sub>4</sub> in the northern winter tropics and extratropics is shown in Fig. 13. Two compact groups of points are

displayed there, one, which is approximately linear, in high latitudes (poleward of 57° N) and one in tropics and subtropics. The same feature also can be found in the Southern Hemisphere and in other seasons. This can be interpreted as the existence of the tropical pipe (Plumb, 1996) in our model.

The lifetime calculated from the model results is 109 yr for N<sub>2</sub>O, 57 yr for F-11 and 95 yr for F-12. Compared with the values of 132 yr for N<sub>2</sub>O, 57 yr for F-11 and 112 for F-12 from AER 2-D CTM without the tropical pipe ( For the detail discussion of the tropical pipe, see Plumb, 1996); and of 103 yr for N<sub>2</sub>O, 45 yr for F-11 and 86 for F-12 with the tropical pipe (Weisenstein, private communication), the three-wave model results are between that of these two CTMs. Because all three models use the same photochemistry, the differences are due to the different residual mean circulations and eddy diffusion coefficients.

## 5.5 Ozone

The O<sub>3</sub> column abundances from the model results and from TOMS data are plotted in Fig. 14 as a function of month and latitude. The ozone column abundance from the baseline model results (Fig. 14 a) shows a strong hemispheric asymmetry. The sources of the asymmetry are the differences of the lower boundary condition for wave generation and the Cunnold (1975) parameterization of tropospheric heating rate in the two hemispheres. These differences in the model inputs generate asymmetry in the model calculated eddy diffusion, the mean meridional transport circulation and the tracer distribution. The general features of the O<sub>3</sub> column distribution are similar to the observations from Total Ozone Mapping Spectrometer (TOMS), which are shown in Fig. 14 b. The modeled spring maximum in both hemispheres appears in the right places with roughly right amplitudes but a little later in time. The calculated ozone column

abundance in the northern mid- and high-latitudes during late summer and fall is about 40-60 Dobson Unit (D. U.) higher than the observations.

It is interesting that the ozone distribution, (Fig. 14 c), calculated using the eddy diffusion coefficient of inert gas ( $K_{yy}^{tot}$  with  $\bar{\gamma}_{ch}=0$ ) for all tracers is quite similar to that using the total eddy diffusion coefficient, (Fig. 14 a). This means that the contribution from the chemical eddy diffusion is not essential in our model. In contrast, the ozone distribution calculated using  $K_{yy}^q$ , (Fig. 14 d), is quite different. Due to larger values of  $K_{yy}^q$ , the ozone maximum in the northern polar spring is 40 D. U. less than observations, but the ozone column abundance in the same region during fall is improved, compared with baseline simulation with  $K_{yy}^{tot}$ .

## 5.6 Correlation Between Ozone and NO<sub>y</sub>

Observations have shown that mixing ratios of O<sub>3</sub> and NO<sub>y</sub> are well correlated in the lower stratosphere (Murphy et al., 1993; Fahey et al., 1996). The ratio of NO<sub>y</sub> to O<sub>3</sub> is nearly independent of altitude from the tropopause to above 20 km. The ratio shows strong meridional gradients in the subtropics. Previous two-dimensional models (e.g., Ko et al., 1993; Solomon and Garcia, 1984) have simulated general features of the vertical profile of NO<sub>y</sub>/O<sub>3</sub> but not the gradient in the lower stratosphere between tropics and mid-latitudes. The mixing ratio of NO<sub>y</sub>, O<sub>3</sub> and their ratio calculated by this model are shown in Fig. 15. The feature of NO<sub>y</sub>/O<sub>3</sub> is very similar to the observation, especially, the strong subtropical meridional gradients are reproduced.

## 6. Discussions

The model reproduces many observed characteristics of dynamics and tracer distributions. The waves are forced by the assigned boundary condition at 850 mb and propagate through the troposphere into the stratosphere. The simulated zonal mean fields and eddies give rise to a reasonable set of residual mean circulation, temperature and eddy diffusion coefficients to the chemistry transport module, which generates distributions for ozone and other long-lived species with desired features. The distributions of long-lived species like N<sub>2</sub>O and CH<sub>4</sub> demonstrate a subtropical transport barrier in the lower stratosphere due to the upward residual circulation in tropics and the small eddy diffusion coefficient in the subtropics. The calculated values for  $K_{yy}^{tot}$  are smaller than  $4 \times 10^5$  (m<sup>2</sup>/sec) from 30° N to 30° S in the lower stratosphere all year around (Fig. 6). Therefore, the tropics is isolated with little exchange between tropics and middle latitudes and acts like a pipe (Plumb, 1996). This also limits the direct exchange between the two hemispheres in the lower stratosphere. The calculated correlation between N<sub>2</sub>O and CH<sub>4</sub> does distinguish the tropical area from the high latitudes.

The total eddy diffusion coefficients for inert tracers ( $K_{yy}^{tot}$  with  $\bar{\gamma}_{ch} = 0$ , shown in Fig. 7), are smaller than the eddy diffusion coefficients derived based on the flux-gradient relationship of potential vorticity,  $K_{yy}^q$ , in our model (Fig. 8). We think that a part of the difference is due to the dissipation of the potential vorticity in our model. In the current version of the model, the dissipation consists of two parts, radiative cooling and friction. With the dissipation, the potential vorticity behaves like a chemically active tracer. Therefore the eddy diffusion coefficients derived from the PV flux-gradient relation include both transient and "chemical" eddy contributions for the PV. Our model calculations show that the dissipation does have a significant contribution to the eddy

diffusion coefficients for PV. Otherwise  $K_{yy}^q$  would be close to the total eddy diffusion coefficients for inert tracers.

Most 2-D CTMs neglect the chemical eddy diffusion and use the same eddy diffusion coefficients for all trace gases. Our model results demonstrate that the chemical eddy diffusion is unimportant in simulating the distribution for most slow species. The mixing ratio of most slow species including ozone,  $N_2O$ ,  $CH_4$ ,  $C_2H_6$ ,  $H_2$ ,  $CO$ ,  $CF_2O$ ,  $NO_y$  and  $Cl_y$  change only less than 10% in most regions and all seasons when chemical eddy diffusion,  $K_{yy}^{ch}$ , is ignored. We think this is the result of competition between the transport and photochemistry. In the region where the chemical eddy diffusion coefficient, which is proportional to the local chemical loss rate,  $\bar{\gamma}$ , is large, the local lifetime ( $1/\bar{\gamma}$ ) of this species must be short and the distribution is mainly determined by the photochemistry not by the transport. In the region where the chemical eddy diffusion coefficient is small the eddy mixing is dominated by the transient eddy and small scale mixing. Therefore, in either case the chemical eddy transport is not essential.

Despite the general agreement between the model simulation and the observations, several aspects of the model results need to be improved. With finer vertical resolution we expect better wave simulation and meridional energy transport to make the lower stratosphere poles warmer during winter. Better representation of the tropospheric heating rates will improve the tropospheric dynamics, the interactions between the stratosphere and troposphere, and the simulation of wave propagation. The calculated ozone column abundance (Fig. 14 a) in the northern high latitudes during fall is about 40 to 60 Dobson Unit higher than observation (Fig. 14 b). We expect that the future improvements of the model (e. g. increasing the number of waves resolved in the model; using finer vertical resolution) will alleviate this problem.

Although the model is built on the primitive equations and other well established equations in physics and chemistry, in order to make the model manageable certain approximations and assumptions have to be applied. The followings are some of the significant assumptions to the model formalism:

- (1) the truncation at  $m = 3$  in the wave expansion and adding the linear damping term in the wave equations to represent dissipation caused by the wave-wave interactions with small waves ( $m > 3$ );
- (2) parameterizations for the tropospheric heating rates, gravity wave dragging (Rayleigh friction), sub-grid diffusion in the latitude direction;
- (3) using family grouping and assuming  $\overline{\gamma' \cdot \chi'} \ll \bar{\gamma} \cdot \bar{\chi}$  in solving zonal mean tracer transport equations;
- (4) ignoring  $S'$  and  $\gamma' \cdot \bar{\chi}$  in the eddy transport equation for tracer;
- (5) assuming that the tracer waves,  $\chi_m(t, y, z)$ , and the velocity waves,  $v_m(t, y, z)$ , have the same decaying rates in calculating  $K_{yy}$ ;
- (6) using a linear damping term in the tracer transport equation to represent mixing by small scale waves.

Most of the approximations and assumptions we used are generally accepted in literature or reasonable. Some of them can be verified in principle as satellite data or 3-D model results become available.

*Acknowledgments.* The support of NASA Office of Mission to Planet Earth Science Division (Contract NASW-4775) is gratefully acknowledged. We would like to thank the anonymous reviewers for their thoughtful comments and suggestions.

## APPENDIX

The data used for the model lower boundary condition and for diagnosis were extracted from an archive of monthly mean grid point analyses of meteorological data, known as the Climate Diagnostics Data Base (CDDDB) (Rasmussen and Arkin, 1985), based on the U. S. National Meteorological Center global analyses, which are generated at 0000 GMT and 1200 GMT daily. The original data were on a  $2.5^\circ$  by  $2.5^\circ$  grid, at nine standard levels in the atmosphere (1000 mb, 850 mb, 700 mb, 500 mb, 300 mb, 250 mb, 200 mb, 100 mb and 50 mb). The data for use in the model consisted of the first seven complex Fourier components interpolated onto the eighteen edges of the 19 bands of latitude used by the model, over the same nine levels.

The original data set spanned the time period from October 1978 to March 1990, and contained values for the zonal component of the wind velocity ( $u$ ), the meridional component ( $v$ ), temperature ( $T$ ), geopotential height ( $\phi$ ), vertical velocity, specific humidity, vorticity and several cross-products. The first step in the extraction process was to create a subset of data from October 1978 to September 1989, which contained  $u$ ,  $v$ ,  $T$  and  $\phi$ , at each of the of the nine pressure levels. The climatological considerations of some of these variables taken from the CDDDB for a similar period, the 1980-89 decade, including estimates of the seasonal and interannual signals, are given by Salstein (1995).

After the spatial series were created, Fourier transforms in space were calculated at each latitude, for each month, variable, and level. The first seven complex harmonics of each transform generated were stored. A climatology was created for the October 1978 to September 1989 period and is used in this study.

Finally, because the model used nineteen bands of latitude, whose edges were defined by eighteen equally spaced latitude circles, and the model required input values along these edges, area weighted averages of the complex Fourier transforms were calculated around each of these latitude circles.

## References

Allen, D. J., A. R. Douglass, and R. B. Rood, 1991: Application of a monotonic upstream transport scheme to three-dimensional constituent transport calculations. *Mon. Wea. Rev.*, **119**, 2456-2464.

Andrews, D. G. and M. E. McIntyre, 1978: Generalized Eliassen-Palm and Charney-Drazin theorems for waves on axisymmetric mean flows in compressible atmospheres, *J. Atmos. Sci.*, **35**, 175-185.

Barnett, J. J., and M. Corney, 1985: Middle atmosphere reference model derived from satellite data. in Handbook for MAP, 16, 47-85, ed. K. Labitzke et al. SCOSTEP Secretariat, Univ. of Illinois, Urbana, Ill.

Bowman, K. P., 1993: Large-scale isentropic mixing properties of Antarctic polar vortex from analyzed winds. *J. Geophys. Res.*, **98**, 23,013-23,023.

Charney, J. G., and P. G. Drazin, 1961: Propagation of planetary-scale disturbances from the lower into the upper atmosphere. *J. Geophys. Res.*, **66**, 83-109.

Choi, W. K. and J. R. Holton, 1991: Transport of N<sub>2</sub>O in the stratosphere related to the equatorial semiannual oscillation. *J. Geophys. Res.*, **96**, 22,543-22,557.

Chen, P., 1994: The permeability of the Antarctic stratosphere., *J. Geophys. Res.*, **99**, 20,563-20,571.

Cunnold, D., F. Alyea, N. Phillips, and R. Prinn, 1975: A three-dimensional dynamical-chemical model of atmospheric ozone. *J. Atmos. Sci.*, **32**, 170-194.

Fahey, D. W., G. D. Donnelly, E. R. Keim, R. S. Gao, R. C. Wamsley, L. A. Del Negro, E. L. Woodbridge, M. H. Proffitt, K. H. Rosenlof, M. K. W. Ko, D. K. Weisenstein, C. J. Scott, C. Nevison, S. Solomon, K. R. Chen, 1996: In situ observations of NO<sub>y</sub> and the NO<sub>y</sub>/O<sub>3</sub> in the lower stratosphere. *Geophys. Res. Lett.* **23**, 1653-1656.

Garcia, R. R., 1991: Parameterization of planetary wave breaking in the middle atmosphere. *J. Atmos. Sci.*, **48**, 1405-1419.

Garcia, R. G., F Strobel, S Solomon, and J. T. Kiehl, 1992: A new numerical model of the middle atmosphere 1. Dynamics and transport of tropospheric source gases. *J. Geophys. Res.*, **97**, 12,967-12,991.

Garcia, R.R., and S. Solomon, 1994: A numerical model of the middle atmosphere 2. Ozone and related species. *J. Geophys. Res.*, **99**, 12,937-12,951.

Hitchman, M. H., and G. Brasseur, 1988: Rossby wave activity in a two-dimensional model: Closure for wave driving and meridional eddy diffusivity. *J. Geophys. Res.*, **93**, 9405-9417.

Kinnersley, J. S. and R. S. Harwood, 1993: An isentropic two-dimensional model with an interactive parameterization of dynamical and chemical planetary-wave fluxes. *Q. J. R. Meteor. Soc.*, **119**, pp. 1167-1193.

Kinnersley, J. S., 1995: A realistic three-component planetary wave model, with a wave-breaking parameterization. *Q. J. R. Meteor. Soc.*, **121**, pp. 853-881.

Ko, M.K.W., N.D. Sze, M. Livshits, M.B. McElroy, and J.A. Pyle, 1984: The seasonal and latitudinal behavior of trace gases and O<sub>3</sub> as simulated by a two-dimensional model of the atmosphere. *J. Atmos. Sci.*, **41**, 2381-2408.

Ko, M.K.W., K.K. Tung, D.K. Weisenstein, and N.D. Sze, 1985: A zonal mean model of stratospheric tracer transport in isentropic coordinates: numerical simulation for nitrous oxide and nitric acid. *J. Geophys. Res.*, **90**, 2313-2329.

Ko, M.K.W., N.D. Sze and D.K. Weisenstein, 1989: The roles of dynamical and chemical processes in determining the stratospheric concentration of ozone in one-dimensional and two-dimensional models. *J. Geophys. Res.*, **94**, 9889-9896.

Ko, M. K. W., H. R. Schneider, R.-L. Shia, D. K. Weisenstein and N.-D. Sze, 1993: A two-dimensional model with coupled dynamics, radiation, and photochemistry: 1. Simulation of the middle atmosphere. *J. Geophys. Res.*, **98**, 20,429-20,440.

Leovy, C. B., C-R. Sun, M. H. Hitchman, E. E. Remsberg, J. M. Russell, III, L. L. Gordley, J. G. Gille and L. V. Lyjak, 1985: Transport of ozone in the middle stratosphere: Evidence for planetary wave breaking. *J. Atmos Sci*, **42**, 230-244.

Matsuno, T., 1980: Lagrangian Motion of air parcels in the stratosphere in the presence of planetary waves. *Pure and Applied Geophys.*, **118**, 189-216.

Murphy, D. M., D. W. Fahey, M. H. Proffitt, S. C. Liu, K. R. Chen, E. S. Eubank, S. R. Kawa, and K. K. Kelly, 1993: Reactive nitrogen and its correlation with ozone in the lower stratosphere and upper troposphere. *J. Geophys. Res.* **98**, 8751-8773.

Newman, P.A., M. R. Schoeberl, R. A. Plumb, and J. E. Rosenfield, 1988: Mixing rates calculated from potential vorticity. *J. Geophys. Res.*, **93**, 5221-5240.

O'Brien, E., and L. Branscome, 1989: Minimal modeling of the extratropical general circulation. *Tellus*, **41A**, 292-307.

Plumb, R. A., 1979: Eddy fluxes of conservative quantities by small-amplitude waves. *J. Atmos. Sci.*, **36** 1699-1704.

Plumb, R. A. and J. D. Mahlman, 1987: The zonally averaged transport characteristics of the GFDL general circulation/transport model. *J. Atmos. Sci.*, **44**, 298-327.

Plumb, R. A., and M.K.W. Ko, 1992: Interrelationships between mixing ratios of long-lived stratospheric constituents. *J. Geophys. Res.*, **97**, 10,145-10,156.

Plumb, R. A., 1996: A "tropical pipe" model of stratospheric transport. *J. Geophys. Res.*, **101**, 3957-3972.

Pyle, J. A. and C. F. Rogers, 1980: Stratospheric transport by stationary planetary waves—the importance of chemical processes. *Quart. J. R. Met. Soc.*, **106**, 421-446.

Rasmussen, E. M. and P. A. Arkin, 1985: Interannual climate variability associated with El Nino/Southern Oscillation, in "Coupled Ocean Atmosphere Models", Elsevier, Amsterdam, 697-725.

Reed, R. J., and K. E. German, 1965: A contribution to the problem of stratospheric diffusion by large-scale mixing. *Mon. Weather Rev.*, **93**, 313-321.

Salstein, D.A., 1995: Mean properties of the atmosphere, Ch.2, in "Composition, Chemistry and Climate of the Atmosphere", van Nostrand Reinhold, New York.

Schneider, H. R. and M. A. Geller, 1984: A comparison of two and three-dimensional transport within a stratospheric circulation model. NASA x-964-84-3.

Schneider, H. R., M. K. W. Ko, R.-L. Shia, and N.-D. Sze, 1993: A two-dimensional model with coupled dynamics, radiative transfer, and photochemistry 2. Assessment of response of stratospheric ozone to increased levels of CO<sub>2</sub>, N<sub>2</sub>O, CH<sub>4</sub>, and CFC. *J. Geophys. Res.*, **98**, 20,441-20,449.

Schoeberl, M. R. and J. T. Bacmeister, 1993: Mixing processes in the extratropical stratosphere. The role of the stratosphere in global change. M. L. Chanin Ed., Springer-Verlag, 135-152.

Shia, R.-L., M. K. W. Ko, M. Zou, and V. R. Kotamarthi, 1993: Cross-tropopause transport of excess <sup>14</sup>C in a two-dimensional model. *J. Geophys. Res.*, **98**, 18,599-18,606.

Smith, A., and G. P. Brasseur, 1990: The dependence of constituent transport on chemistry in a two-dimensional model of the middle atmosphere. *J. Geophys. Res.*, **95**, 13,749-13,764.

Solomon, S., and R. R. Garcia, 1984: On the distribution of long-lived tracers and chlorine species in the middle atmosphere. *J. Geophys. Res.*, **89**, 11,633-11,644.

Strobel, D. F., 1981: Parameterization of linear wave chemical transport in planetary atmospheres by eddy diffusion. *J. Geophys. Res.*, **86**, 9806-9810.

Tuck, A. F., J. M. Russell III, and J. E. Harries, 1993: Stratospheric dryness: Antiphased desiccation over Micronesia and Antarctica. *Geophys. Res. Lett.*, **20**, pp. 1227-1230.

Tung, K. K., 1984: Modeling of tracer transport in the middle atmosphere. Dynamics of the middle atmosphere. J. R. Holton and T. Matsuno, Eds., Terra Scientific, 412-444.

Tung, K. K., 1987: A coupled model of zonally averaged dynamics, radiation and chemistry. in Transport processes in the middle atmosphere. G. Visconti and R. R. Garcia, Eds., 183-198.

Wang, W.-C. and P. B. Ryan, 1983: Overlapping effect of atmospheric H<sub>2</sub>O, CO<sub>2</sub> and O<sub>3</sub> on the CO<sub>2</sub> radiative effect. *Tellus*, **35B**, 81-91.

Waugh, D. W., R. A. Plumb, 1994: Contour advection with surgery: A technique for investigating fine scale structure in tracer transport. *J. Atmos. Sci.*, **51**, 530-540.

Weissenstein, D. K., M. K. W. Ko, J. M. Rodriguez and N.-D. Sze, 1993: Effects on stratospheric ozone from High-Speed Civil Transport: Sensitivity to stratospheric aerosol loading. *J. Geophys. Res.*, **98**, 23,133-23140.

Yang, H., E. Olaguer, and K. K. Tung, 1991: Simulation of the present-day atmospheric ozone, odd nitrogen, chlorine and other species using a coupled 2-D model in isentropic coordinates, accepted by *J. Atmos. Sci.*, **48**, 442-471.

Zhou, S., and P. H. Stone, 1993: The role of large-scale eddies in the climate equilibrium. Part I: Fixed static stability. *J. Climate*, **6**, 985-1001.

## Figure captions

Fig. 1 The flow chart of the three-wave interactive model. The arrows indicate the direction of data flow. The loops formed by arrows represent feedbacks.

Fig. 2 The prescribed wave amplitude in the model's lower boundary, for (a). January and (b). July respectively. The solid lines is for wave 1, dash line for wave 2, and dot line for wave 3.

Fig. 3 The model calculated mean zonal wind,  $\bar{u}$ , and temperature,  $\bar{T}$ , (a).  $\bar{u}$  in January, (b).  $\bar{T}$  in January, (c).  $\bar{u}$  in July, and (d).  $\bar{T}$  in July. The contour interval is 10 m/s for  $\bar{u}$  and 10° for  $\bar{T}$ .

Fig. 4 Comparison of the model results and the observations for the wave amplitude of geopotential height. (a) January; (b) July. The contour increments are 40 m, 20 m, and 10 m for wave 1, 2, and 3 respectively.

Fig. 5 The calculated streamfunction of the residual circulation,  $\psi$ , for (a) January, (b) April, (c) July, and (d) October. The contours plotted are -2, -1, -0.5, -0.2, -0.1, -0.05, -0.02, -0.01, -0.005, 0, 0.005, 0.01, 0.02, 0.05, 0.1, 0.2, 0.5, 1, 2  $\times (10^{-8} \text{ km}^2/\text{s})$ . The values correspond the meridional mass flux scaled by  $(A \rho_s)$ , where  $A$  is the radius of the Earth and  $\rho_s$  is the surface air density.

Fig. 6 The total eddy diffusion coefficient,  $K_{yy}^{tot}$ , ( $10^6 \text{ m}^2/\text{sec}$ ) for ozone, in (a) January, (b) April, (c) July, and (d) October. The contour levels are 0, .05, 0.1, 0.2, 0.4, 0.8, 1.0 and 1.5. The areas with negative values are shaded. The calculated  $K_{yy}^{tot}$  is plotted for

whole model region. In the model, a constant value of  $K_{yy}$  is added in the troposphere to simulate rapid mixing in the troposphere.

Fig. 7 Same as Fig. 6, but for inert tracer ( $K_{yy}^{tot}$  with  $\bar{\gamma}_{ch} = 0$ ).

Fig. 8 Same as Fig. 6 but for eddy diffusion coefficient derived based on PV flux-gradient relation,  $K_{yy}^q$ . The comparisons of  $K_{yy}^q$  with the total eddy diffusion coefficient,  $K_{yy}^{tot}$ , for ozone shown in Fig. 6 or for inert tracer shown in Fig. 7 should be limited in the stratosphere.

Fig. 9 Latitude-altitude cross section of calculated N<sub>2</sub>O mixing ratio (ppbv) for (a) January, (b) April, (c) July, and (d) October. The contour levels are 5, 10, 25, 50, 100, 150, 200, 250, and 300 ppbv.

Fig. 10 Latitude-altitude cross section of calculated CH<sub>4</sub> mixing ratio (ppmv) for (a) January, (b) April, (c) July, and (d) October. The contour increment is 0.2 ppmv.

Fig. 11 The Monthly averaged zonal mean of (a) UARS/CLAES N<sub>2</sub>O for March of 1993, and (b) UARS/CLAES CH<sub>4</sub> for March of 1993. Archived data are from UARS CD-ROM Vol. 7.

Fig. 12 Same as Fig. 10, but using eddy diffusion coefficient derived based on PV flux-gradient relation,  $K_{yy}^q$ , instead of  $K_{yy}^{tot}$ .

Fig. 13 The correlation of N<sub>2</sub>O and CH<sub>4</sub> mixing ratio (a) in the northern mid-high latitudes, and (b) in the tropics. A straight line is

added in each panel to show that the transport characters in the tropics and in the high latitudes are different (Plumb and Ko, 1992).

Fig. 14 Latitude-time cross section of ozone column abundance (D. U.) from (a). model calculation, (b). TOMS measurements, (c). same as (a) but using the eddy diffusion coefficient for inert tracer ( $K_{yy}^{tot}$  with  $\bar{y}_{ch} = 0$ ), for all trace gases, and (d). same as (a) but using eddy diffusion coefficient derived based on PV flux-gradient relation,  $K_{yy}^q$ , for all trace gases instead of  $K_{yy}^{tot}$ . The contour increment is 20 D. U.

Fig. 15 The mixing ratio of (a)  $\text{NO}_y$  and (b)  $\text{O}_3$ , as well as (c) their ratio,  $\text{NO}_y/\text{O}_3$  along with the AAOE, STEP, and AASE data (Murphy et al., 1993) in the lower stratosphere (64 mb), in January.



# 3-Wave Interactive Model

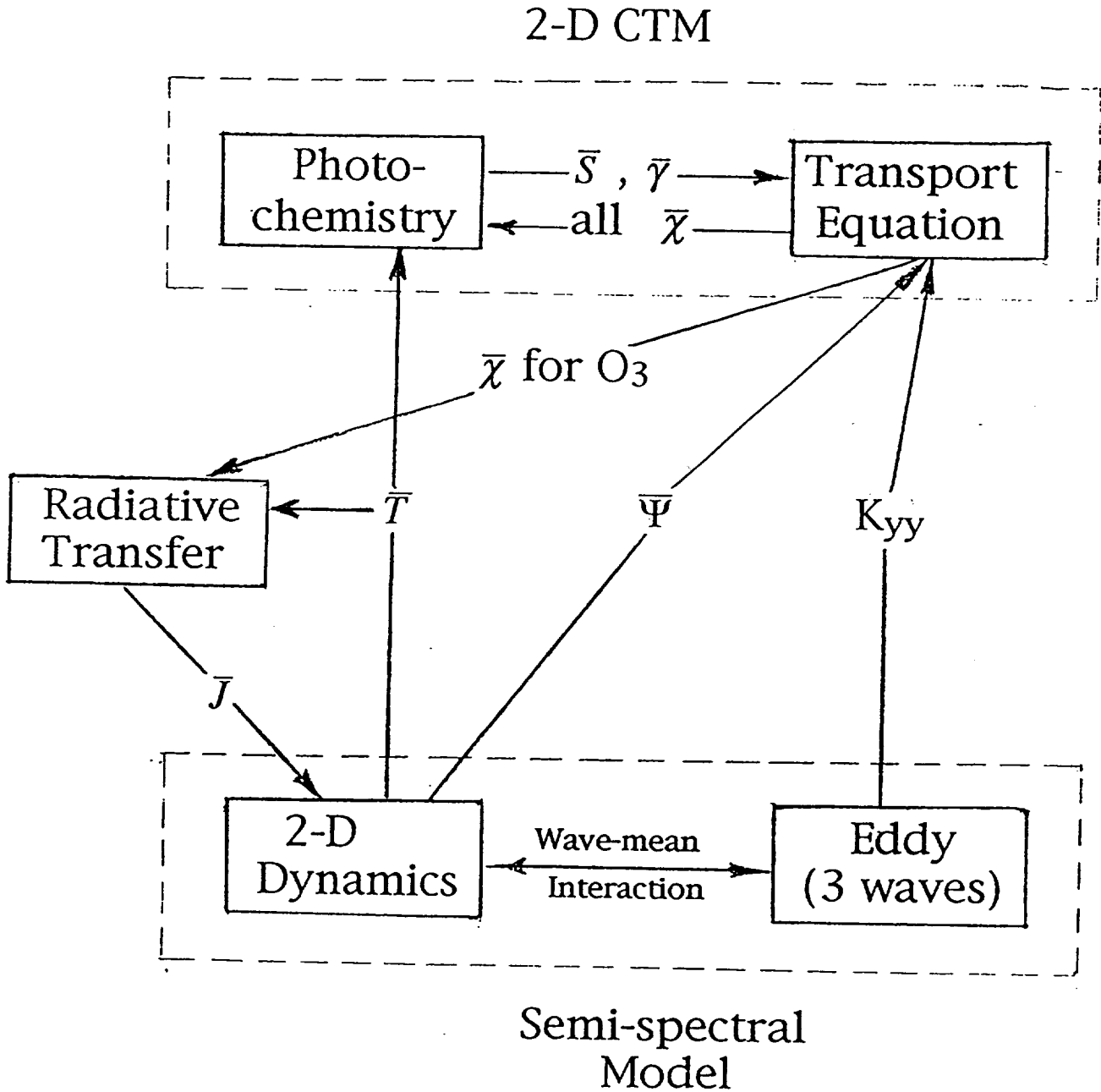


Fig. 1 The flow chart of the three-wave interactive model. The arrows indicate the direction of data flow. The loops formed by arrows represent feedbacks.

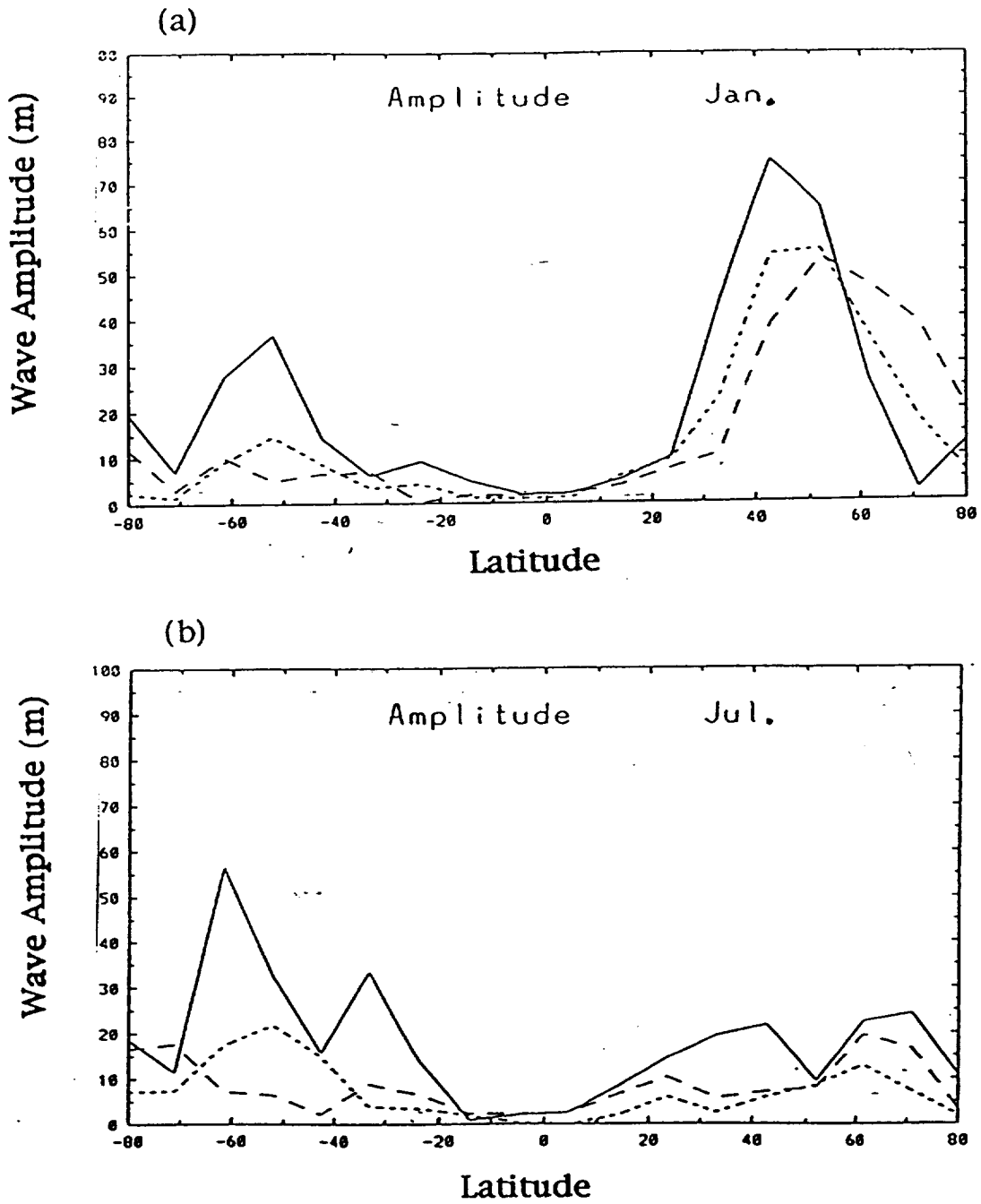
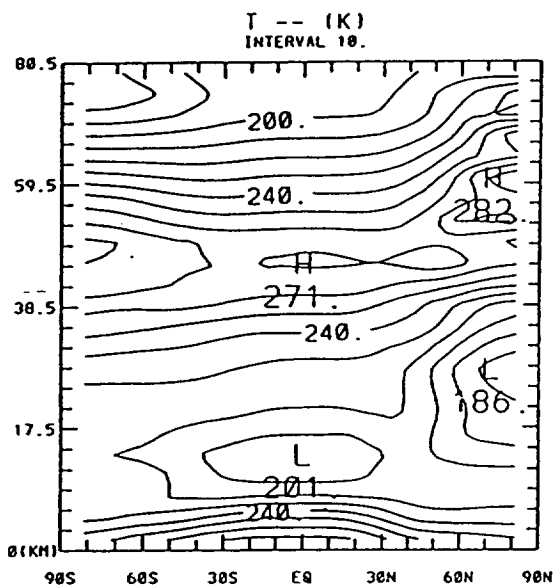
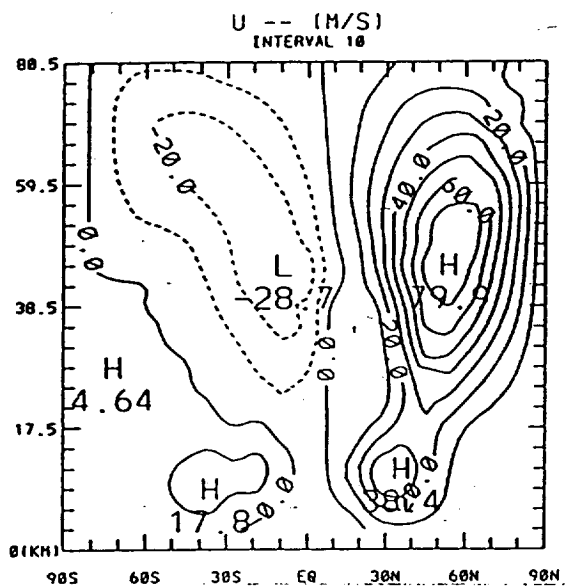


Fig. 2 The prescribed wave amplitude in the model's lower boundary, for (a). January and (b). July respectively. The solid lines is for wave 1, dash line for wave 2, and dot line for wave 3.

(a)



(b)

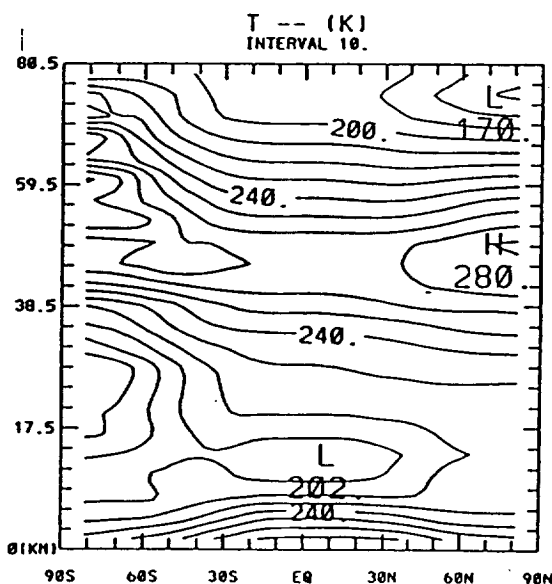
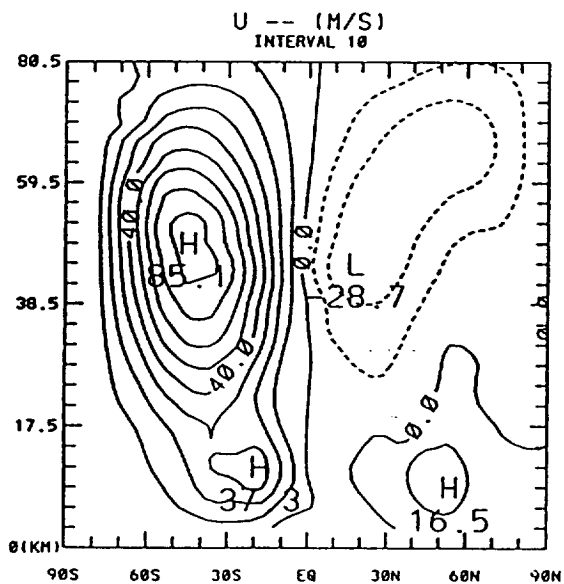


Fig. 3 The model calculated mean zonal wind  $\bar{u}$ , and temperature,  $\bar{T}$ , (a).  $\bar{u}$  in January, (b).  $\bar{T}$  in January, (c).  $\bar{u}$  in July, and (d).  $\bar{T}$  in July. The contour interval is 10 m/s for  $\bar{u}$  and 10° for  $\bar{T}$ .

# Wave Amplitude (m)

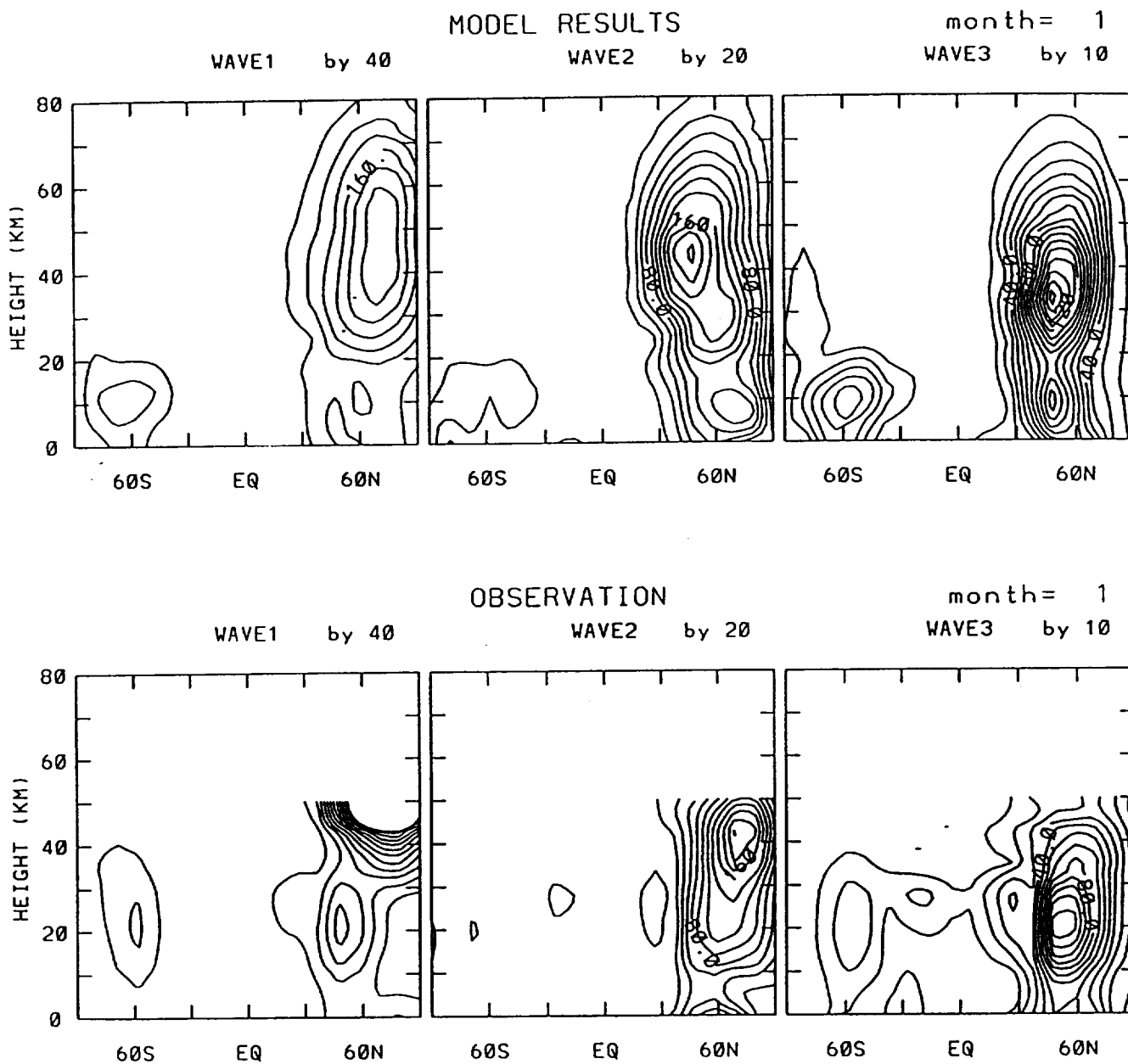


Fig. 4 (a). Comparison of the model results and the observations for the wave amplitude of geopotential height for January. The contour increments are 40 m, 20 m, and 10 m for wave 1, 2, and 3 respectively.

# Wave Amplitude (m)

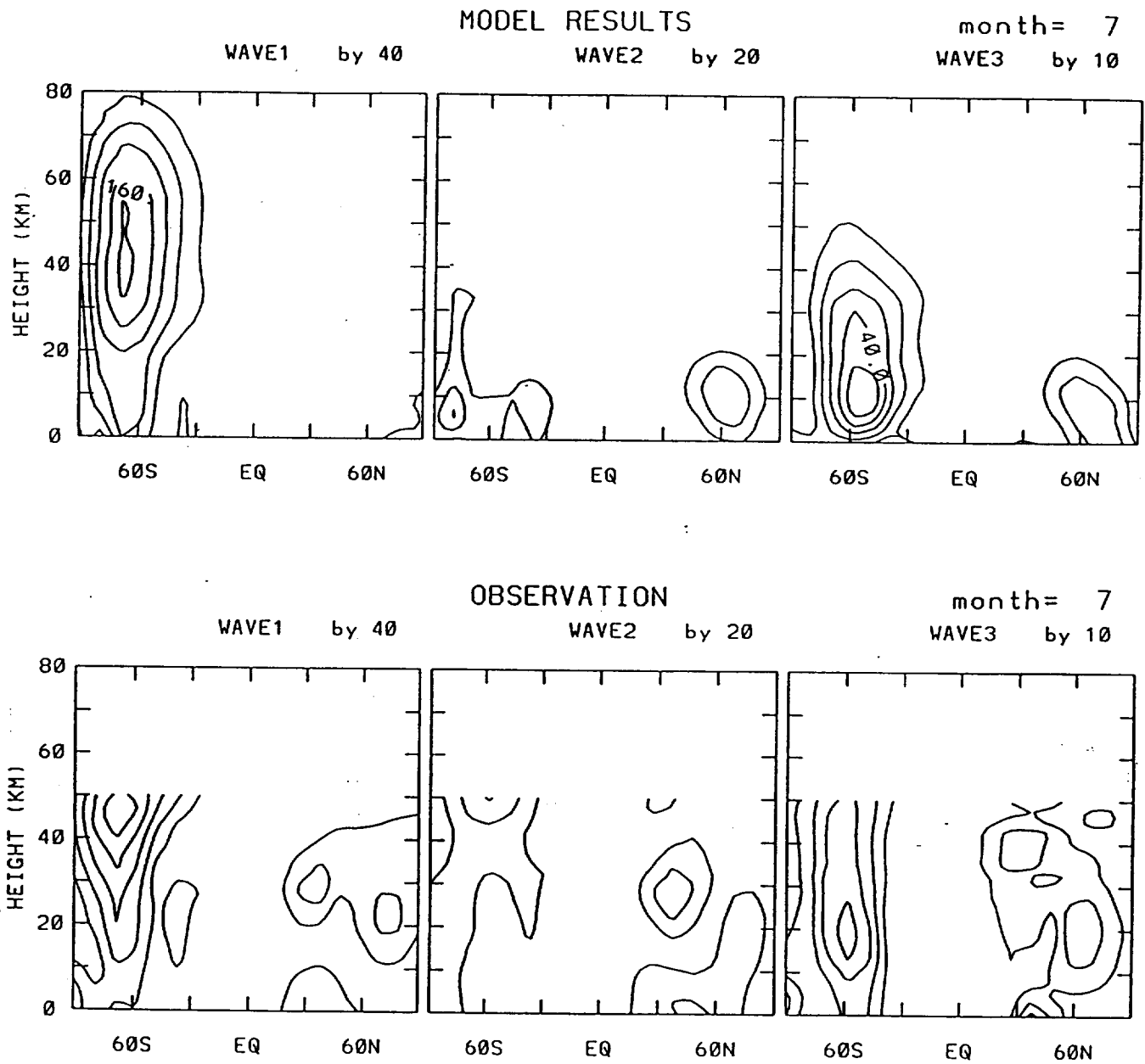


Fig. 4 (b). The same as Fig. 4 (a) but for July.

PSI

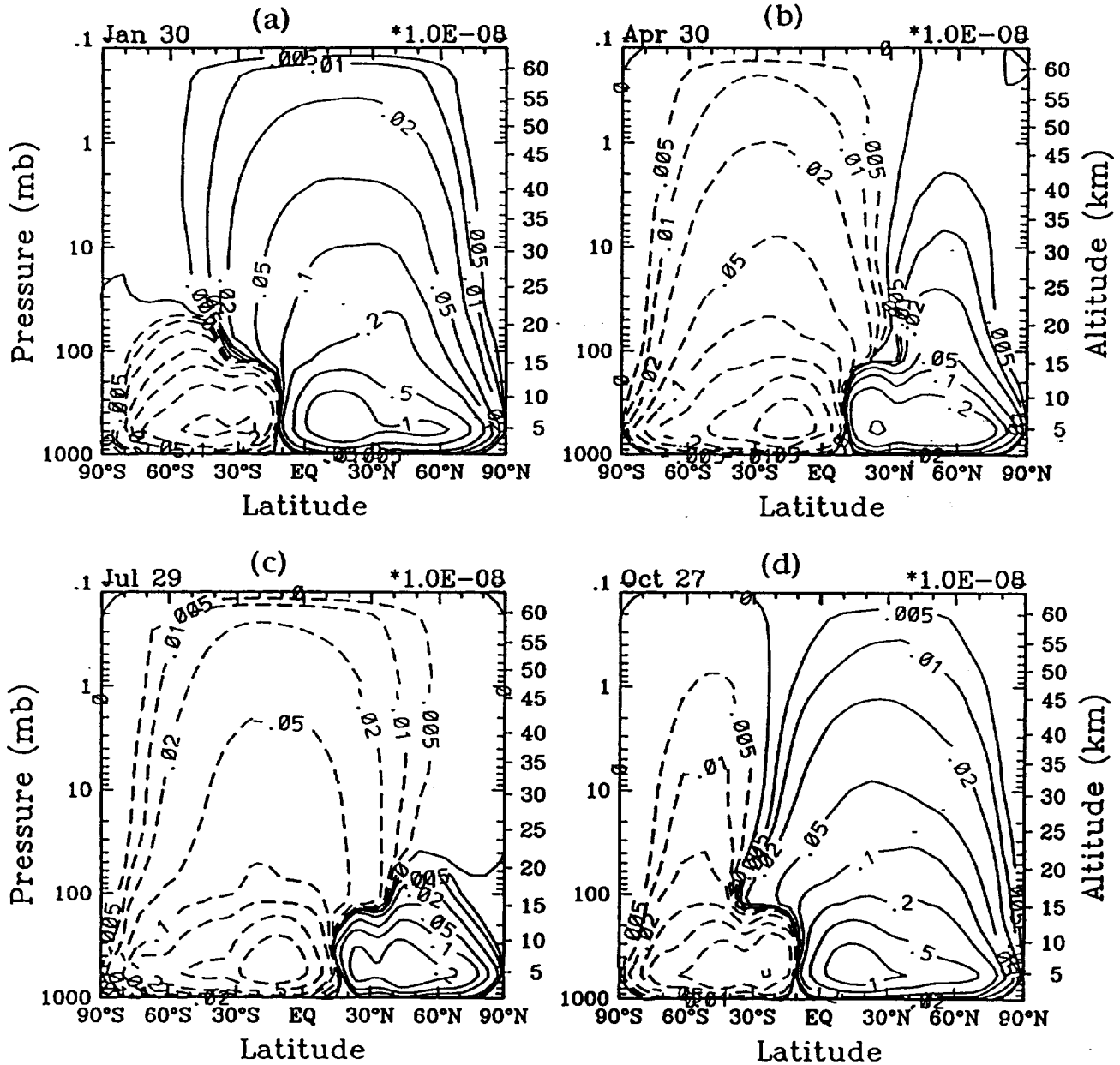


Fig. 5 The calculated streamfunction of the residual circulation,  $\psi$ , for (a) January, (b) April, (c) July, and (d) October. The contours plotted are -2, -1, -0.5, -0.2, -0.1, -0.05, -0.02, -0.01, -0.005, 0, 0.005, 0.01, 0.02, 0.05, 0.1, 0.2, 0.5, 1, 2  $\times (10^{-8} \text{ km}^2/\text{s})$ . The values correspond the meridional mass flux scaled by  $(A\rho_s)$ , where  $A$  is the radius of the Earth and  $\rho_s$  is the surface air density.

Kyy(03)

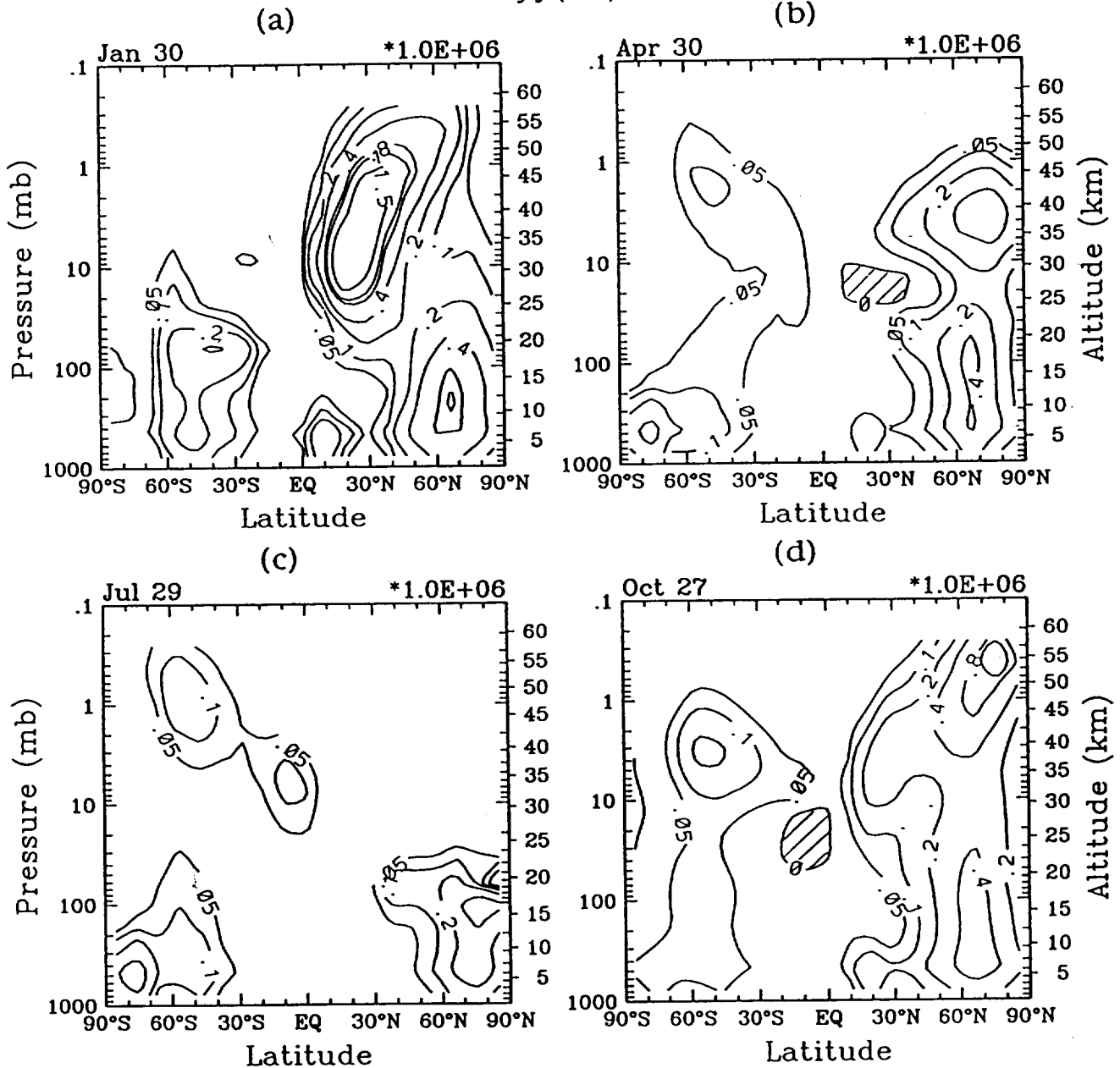


Fig. 6 The total eddy diffusion coefficient,  $K_{yy}^{tot}$ , ( $10^6 \text{ m}^2/\text{sec}$ ) for ozone, in (a) January, (b) April, (c) July, and (d) October. The contour levels are 0, .05, 0.1, 0.2, 0.4, 0.8, 1.0 and 1.5. The areas with negative values are shaded. The calculated  $K_{yy}^{tot}$  is plotted for whole model region. In the model, a constant value of  $K_{yy}$  is added in the troposphere to simulate rapid mixing in the troposphere.

Kyy for inert tracer

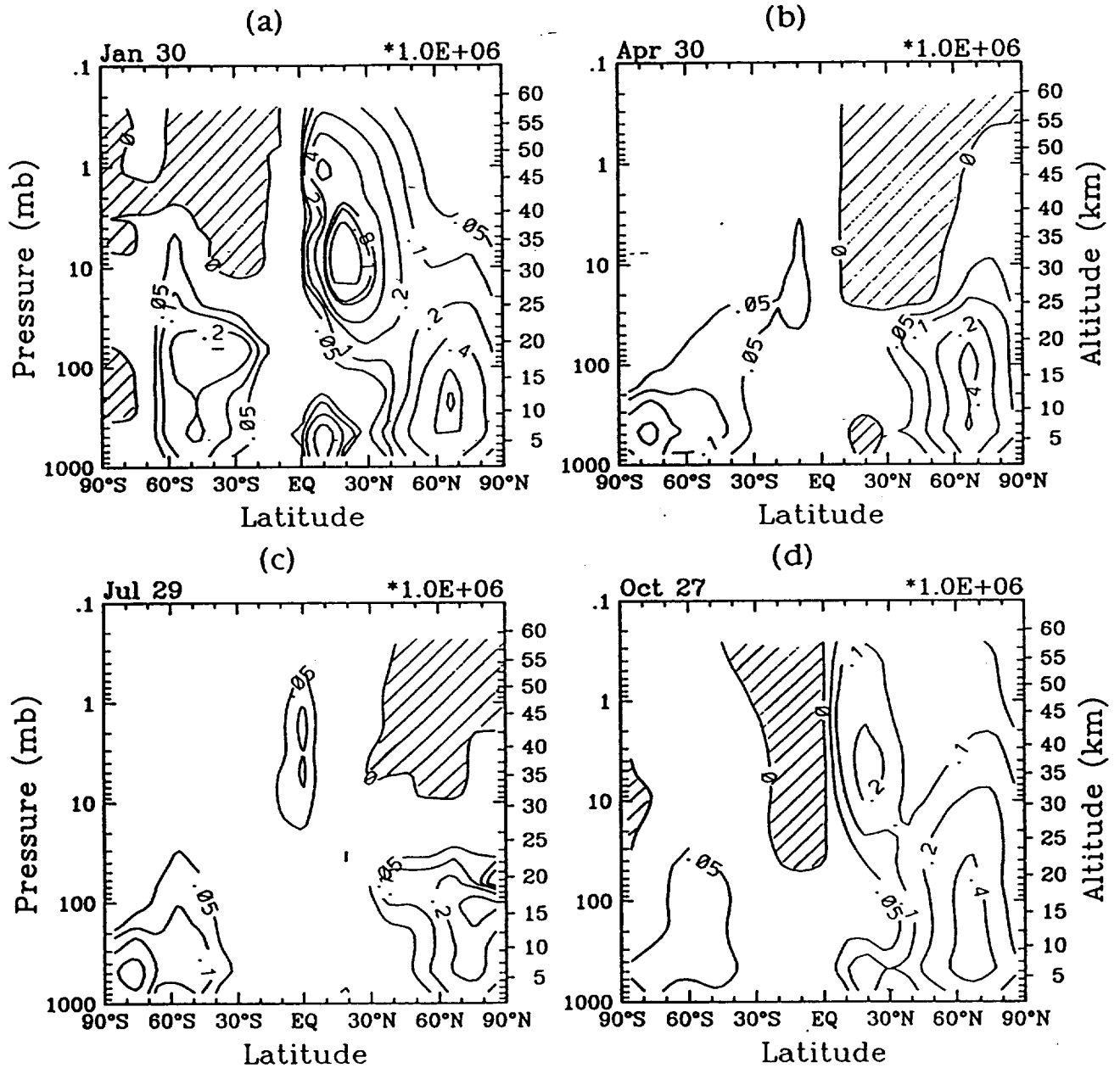


Fig. 7 Same as Fig. 6, but for inert tracer ( $K_y^{tot}$  with  $\bar{\gamma}_{ca} = 0$ ).

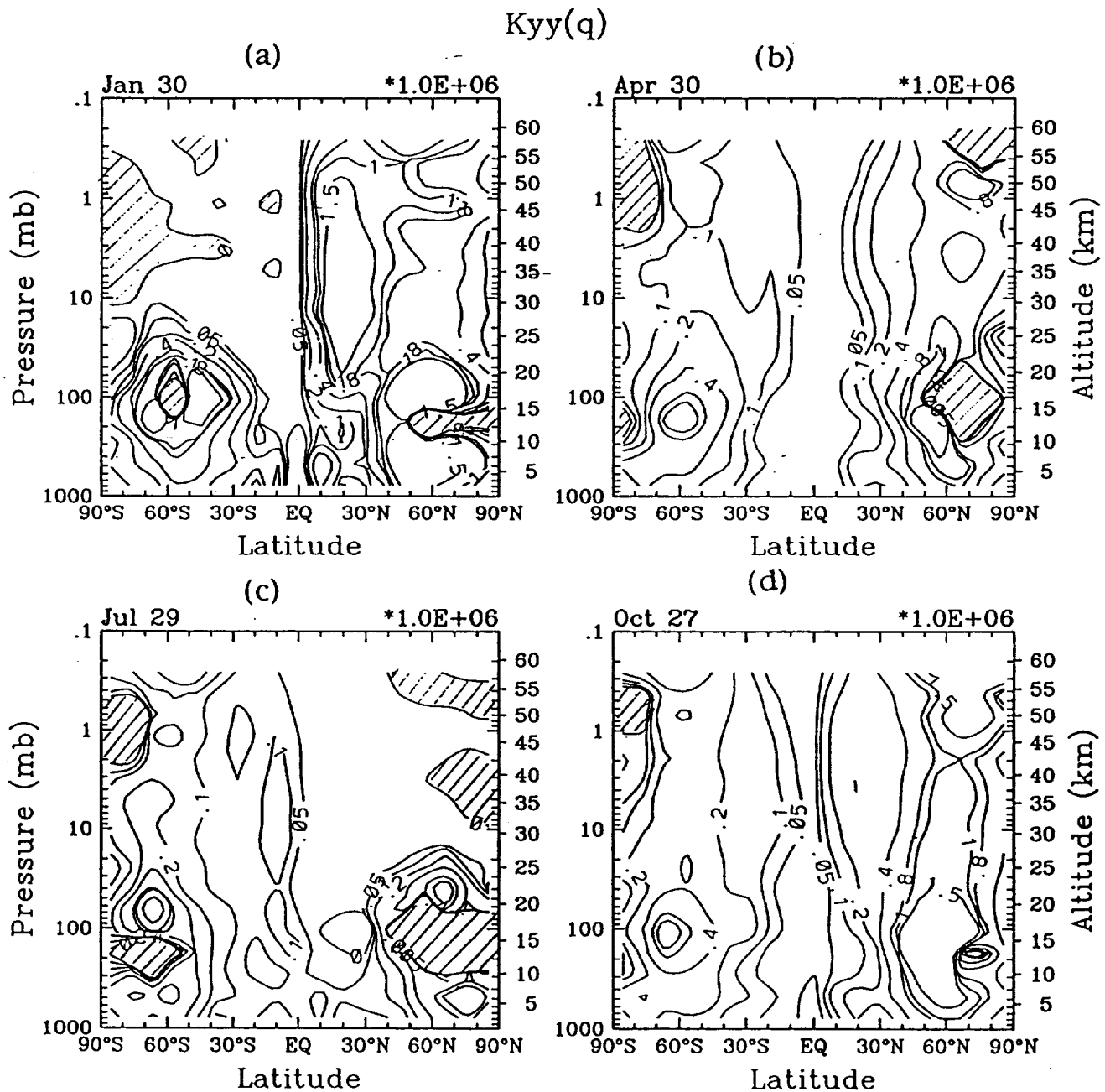


Fig. 8 Same as Fig. 6 but for eddy diffusion coefficient derived based on PV flux-gradient relation,  $K_{yy}^q$ . The comparisons of  $K_{yy}^q$  with the total eddy diffusion coefficient,  $K_{yy}^{tot}$ , for ozone shown in Fig. 6 or for inert tracer shown in Fig. 7 should be limited in the stratosphere.

N2O

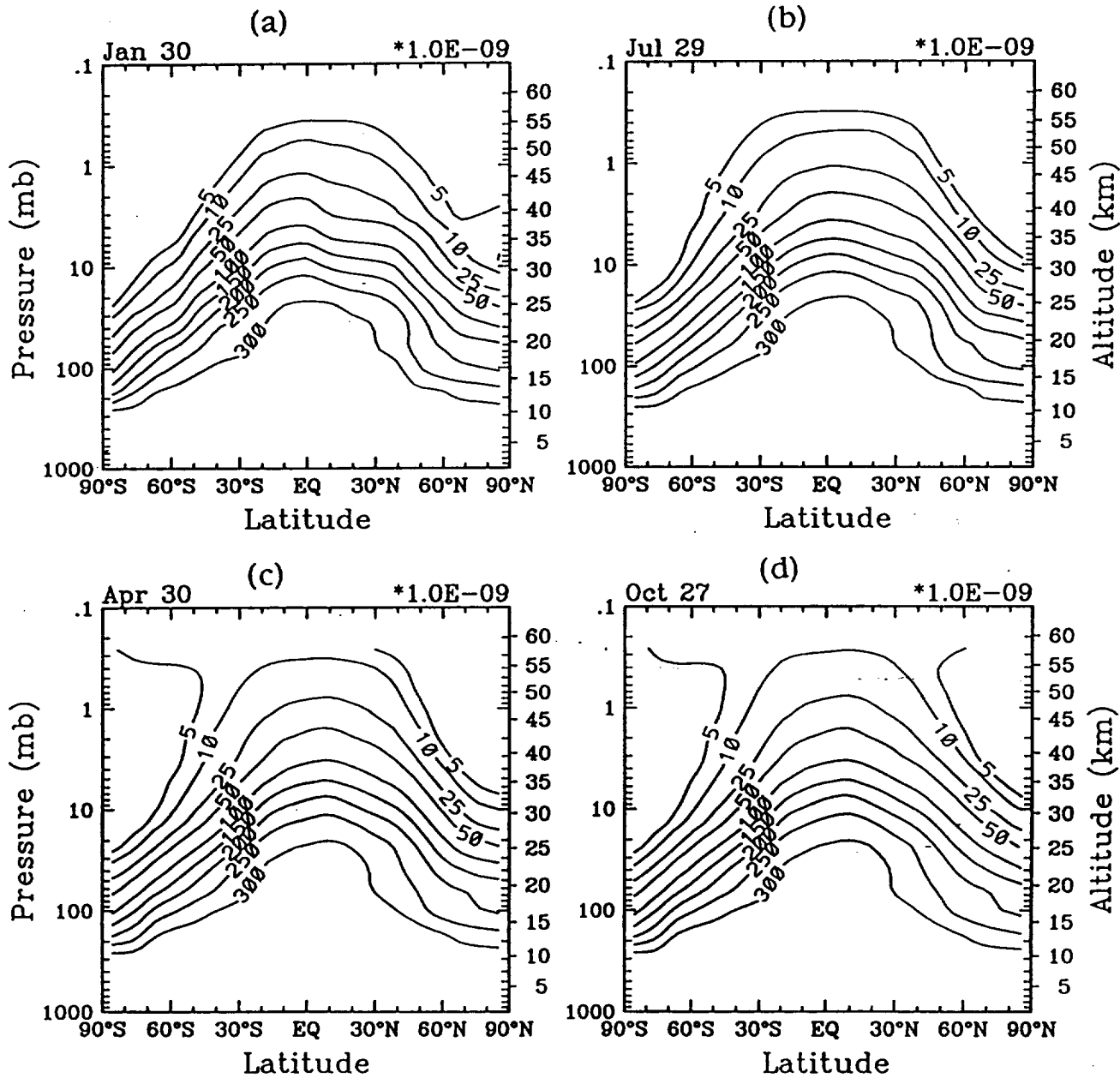


Fig. 9 Latitude-altitude cross section of calculated N<sub>2</sub>O mixing ratio (ppbv) for (a) January, (b) April, (c) July, and (d) October. The contour levels are 5, 10, 25, 50, 100, 150, 200, 250, and 300 ppbv.

CH4

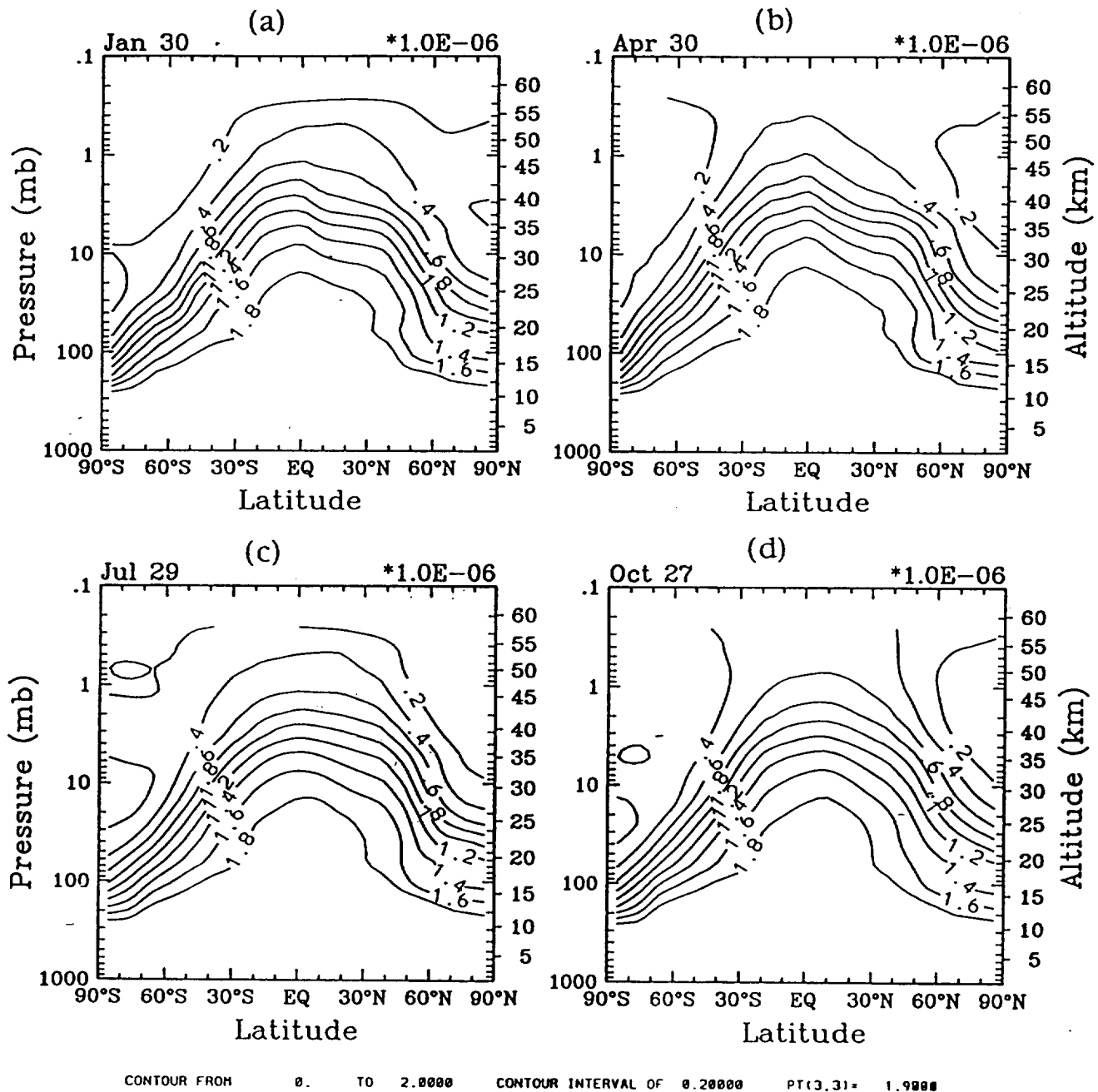


Fig. 10 Latitude-altitude cross section of calculated CH<sub>4</sub> mixing ratio (ppmv) for (a) January, (b) April, (c) July, and (d) October. The contour increment is 0.2 ppmv.

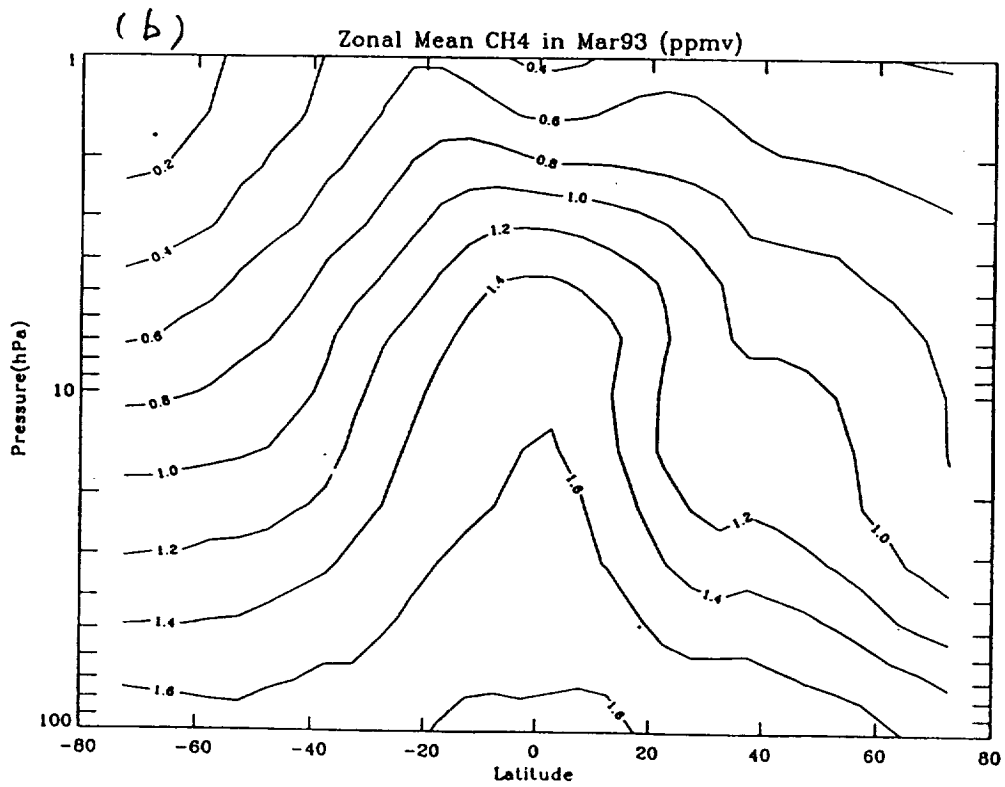
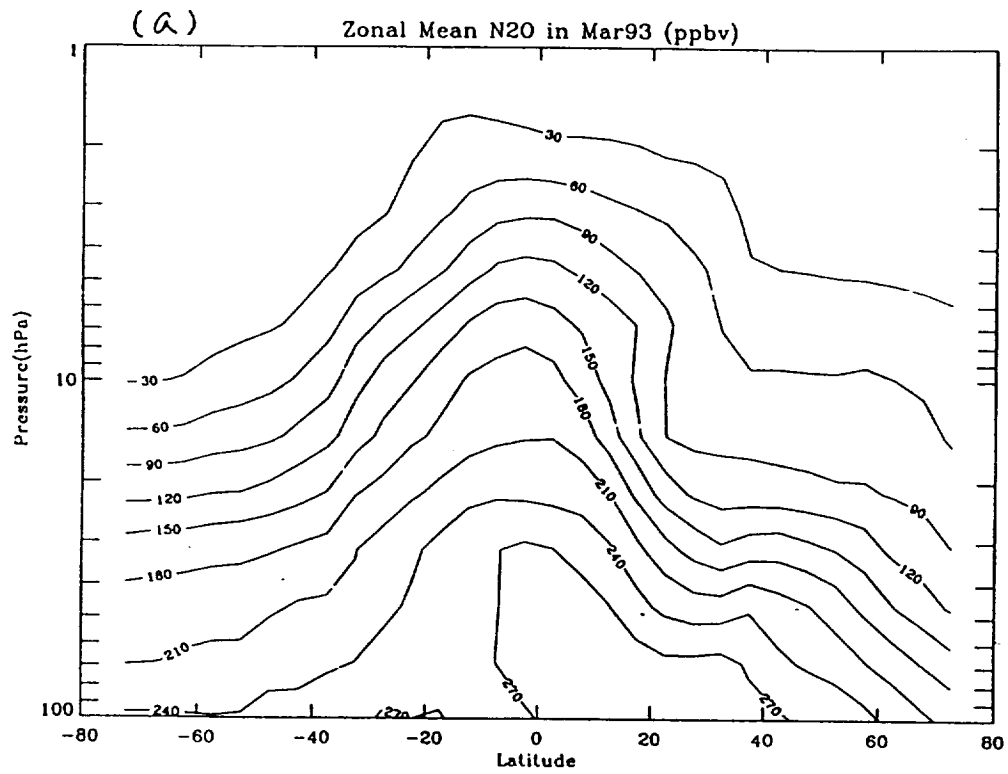
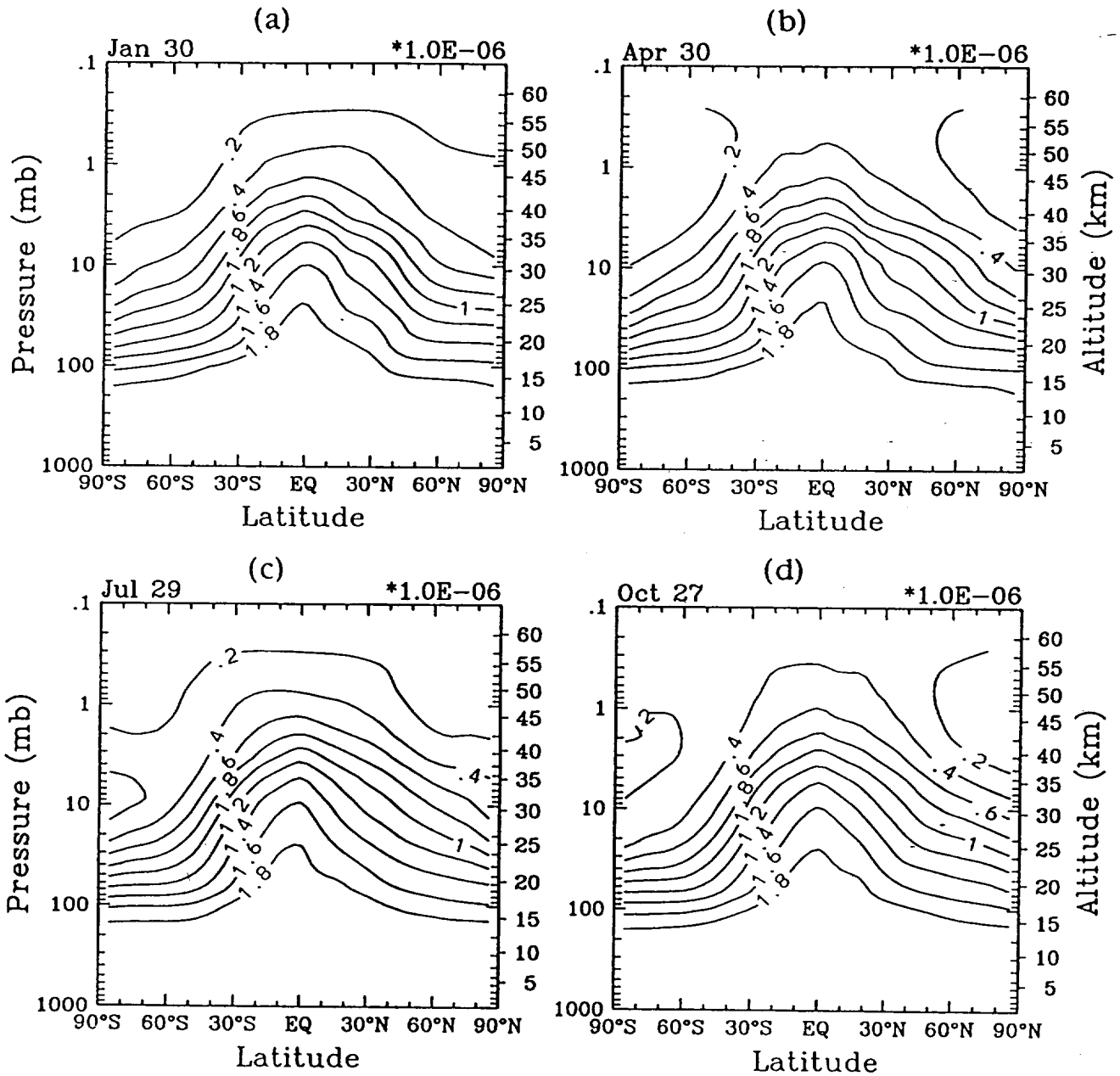


Fig. 11 The Monthly averaged zonal mean of (a) UARS/CLAES N<sub>2</sub>O for March of 1993, and (b) UARS/CLAES CH<sub>4</sub> for March of 1993. Archived data are from UARS CD-ROM Vol. 7.

CH4



CONTOUR FROM 0. TO 2.0000 CONTOUR INTERVAL OF 0.20000 PT(3,3)= 1.9888

Fig. 12 Same as Fig. 11, but using eddy diffusion coefficient derived based on PV flux-gradient relation,  $K_{yy}^e$ , instead of  $K_{yy}^{tot}$ .

# $N_2O-CH_4$ Correlation for Jan

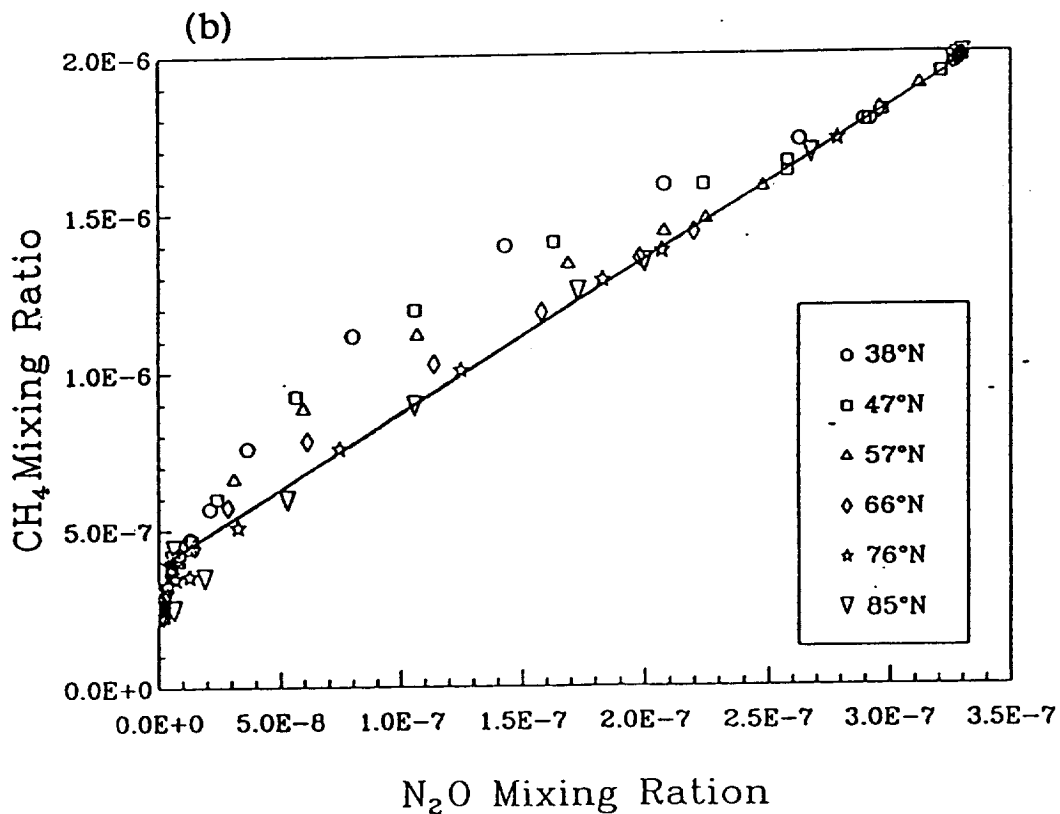
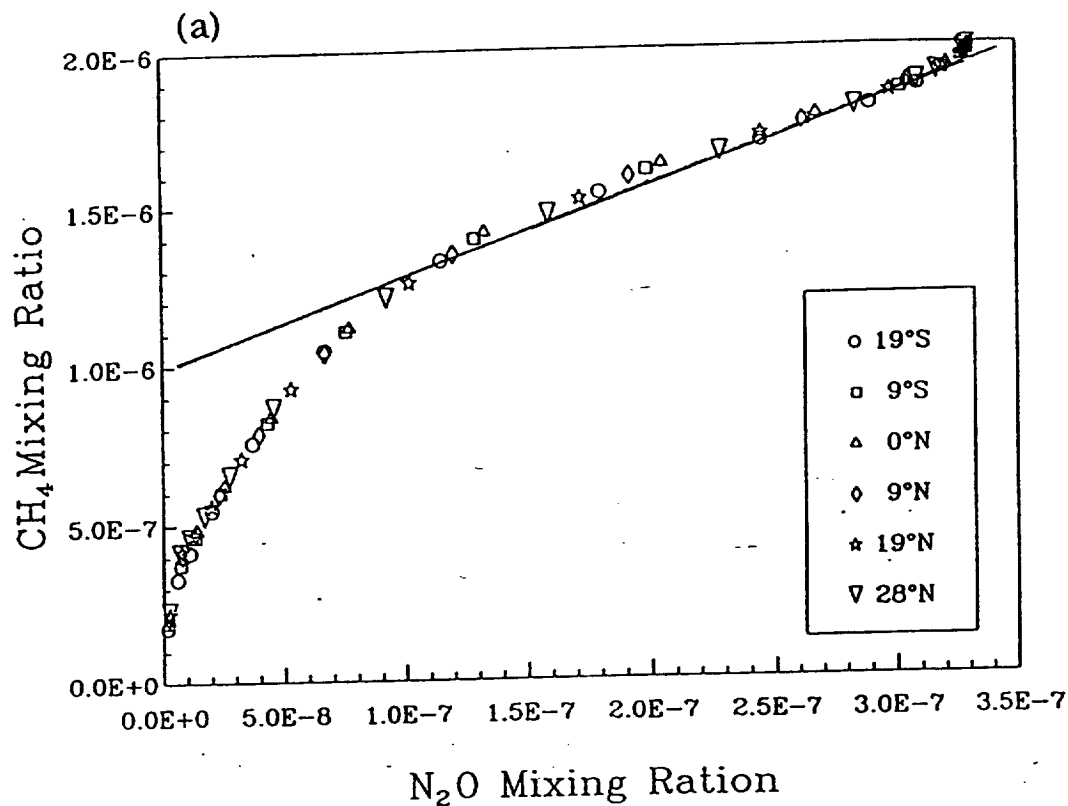


Fig. 13 The correlation of  $N_2O$  and  $CH_4$  mixing ratio (a) in the northern mid-high latitudes, and (b) in the tropics. A straight line is added in each panel to show that the transport characters in the tropics and in the high latitudes are different (Plumb and Ko, 1992).

## Ozone Column Abundance (D. U.)

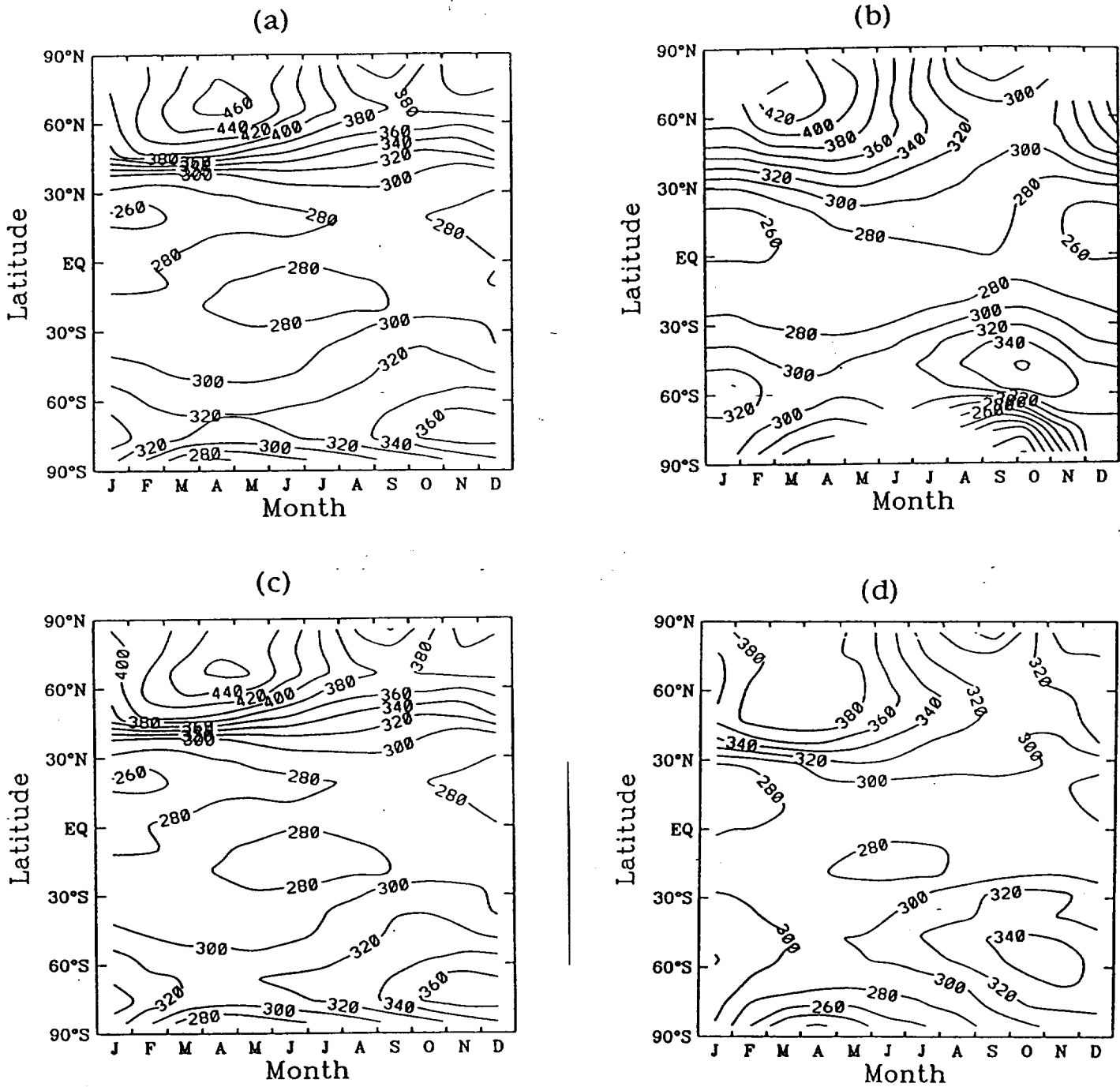


Fig. 14 Latitude-time cross section of ozone column abundance (D. U.) from (a). model calculation, (b). TOMS measurements, (c). same as (a) but using the eddy diffusion coefficient for inert tracer ( $K_{yy}^{tot}$  with  $\bar{\gamma}_{ch} = 0$ ), for all trace gases, and (d). same as (a) but using eddy diffusion coefficient derived based on PV flux-gradient relation,  $K_{yy}^e$ , for all trace gases instead of  $K_{yy}^{tot}$ . The contour increment is 20 D. U.

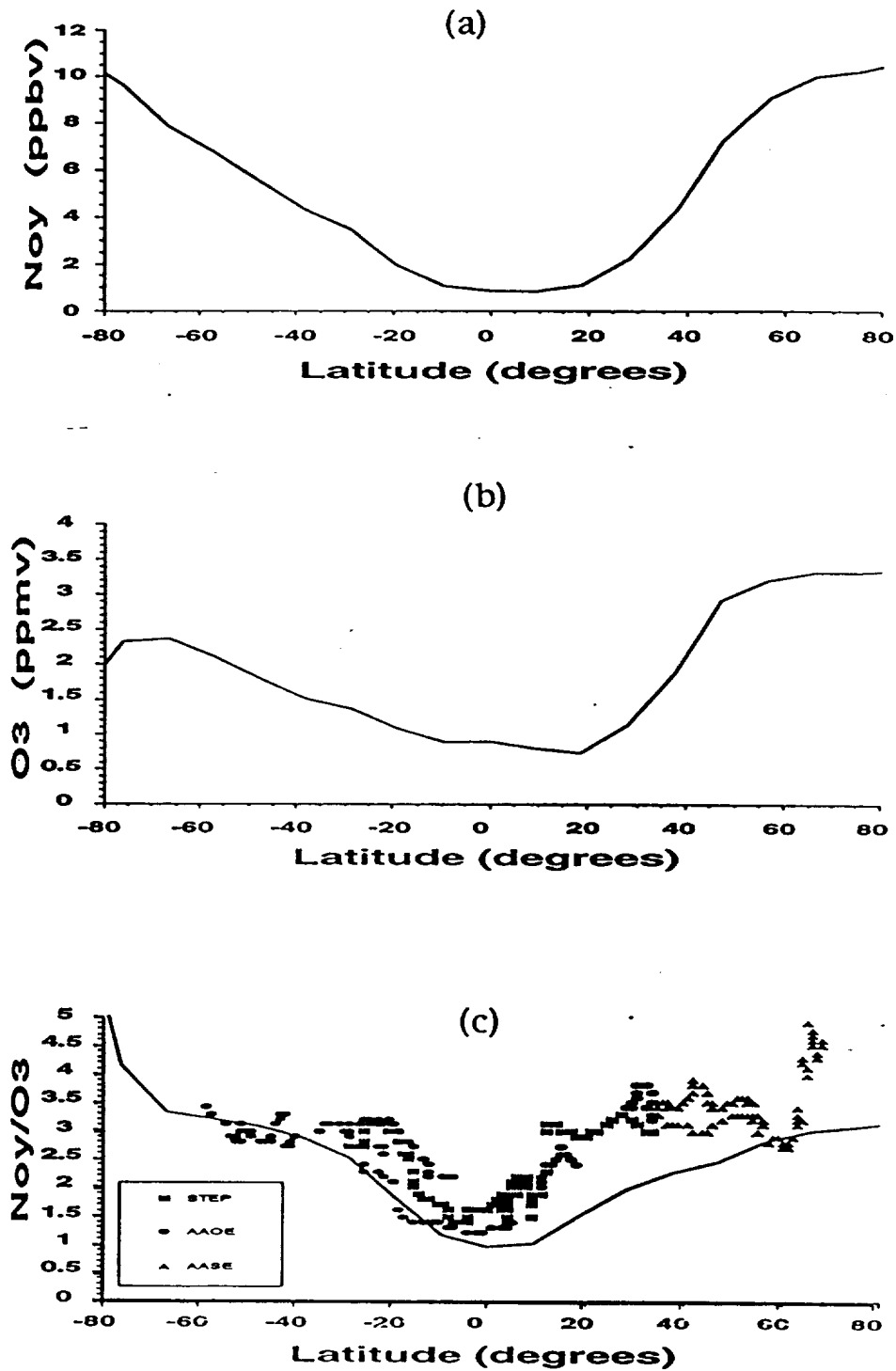


Fig. 15 The mixing ratio of (a) NO<sub>y</sub> and (b) O<sub>3</sub>, as well as (c) their ratio, NO<sub>y</sub>/O<sub>3</sub> along with the AAOE, STEP, and AASE data (Murphy et al., 1993) in the lower stratosphere (64 mb), in January.